P-11-30

Acoustic emission and ultrasonic monitoring results from deposition hole DA3545G01 in the Prototype Repository between April 2009 and September 2009

Jon Haycox, Will Pettitt
ASC, Applied Seismology Consultants

December 2009

Svensk Kärnbränslehantering AB
Swedish Nuclear Fuel
and Waste Management Co

Box 250, SE-101 24 Stockholm
Phone +46 8 459 84 00

ISSN 1651-4416
SKB P-11-30
ID 1289011

Acoustic emission and ultrasonic monitoring results from deposition hole DA3545G01 in the Prototype Repository between April 2009 and September 2009

Jon Haycox, Will Pettitt
ASC, Applied Seismology Consultants

December 2009

Executive summary

This report describes the results from acoustic emission (AE) and ultrasonic monitoring around a canister deposition hole (DA3545G01) in the Prototype Repository Experiment at SKB's Hard Rock Laboratory (HRL), Sweden. The monitoring aims to examine changes in the rock mass caused by an experimental repository environment, in particular due to thermal stresses induced from canister heating and pore pressure variation induced from tunnel sealing. Monitoring of this volume has been performed during excavation and for six years during stages of canister heating and tunnel pressurisation.

Two techniques are utilised here to investigate the processes occurring within the rock mass around the deposition hole: ultrasonic survey and acoustic emission monitoring. Ultrasonic surveys are used to 'actively' examine the rock. Velocity changes are measured between transmitter-receiver pairs using a cross-correlation technique that allows a velocity resolution of ± 2 ms^{-1}. Amplitude and velocity changes on the ray-paths can then be interpreted in terms of changes in the material properties of the rock. Calculations using the velocities can determine the changes in dynamic moduli, Young's modulus and Poisson's ratio, to give direct indications of the properties of the rock through which the ray-paths travel. Crack density and saturation can also be calculated to determine changes in crack properties in the damaged and disturbed zones. AE monitoring is a 'passive' technique similar to earthquake monitoring but on a much smaller distance scale (source dimensions of millimetres). AEs occur on fractures in the rock when they are created or when they propagate.

Ultrasonic monitoring has been conducted at the Prototype Repository since September 1999. During excavation, monitoring of both deposition holes in Section 2 of the Prototype Tunnel was undertaken to delineate zones of stress-related fracturing and quantitatively measure fracturing in the damaged zone. A permanent ultrasonic array was installed in the rock-mass in June 2002 around deposition hole DA3545G01.

This report covers the period between 1st April 2009 and 30th September 2009 and is the ninth 6-monthly processing and interpretation of the results from the experiment. Temperature of the rock surrounding deposition hole DA3545G01 is very stable during this period, and pressure around the deposition hole and in the backfill above the deposition hole has observed a steady increase. Ultrasonic surveying was not possible for transmitters 2 to 8 (inclusive) between 28th August 2009 and the end of the reporting period due to equipment malfunction. The malfunction was fixed on 4th November 2009.

During this monitoring period there were a total of 25 AE events located with high confidence (Figure ES-1). A study of the spatial distribution of AEs shows that the majority of events are associated with distinct clusters. A peak in activity on 8th June 2009 is associated with events positioning in two clusters, labelled E and F, where significant activity has not been observed since deposition hole excavation. Cluster E is located towards the bottom, and on the south west side of the deposition hole in a region characterised by high compressive stress. Cluster F is positioned in a region where events have not been previously located by the AE system but are close (30 cm) to event clusters recorded during excavation. The events are close to the tunnel, in a region characterised by high compressive stress; possibly a zone that was damaged during tunnel excavation. The events in Clusters B, C and D are located in the same volumes as clusters observed in previous monitoring periods and are thus interpreted as occurring along the same structures. The events could be a continuation of activity in the damaged zone, created either by movement on pre-existing microcracks or as a result of extension or formation of new microcracks in the existing damaged region. Therefore we can assume that the rock mass around the deposition holes has remained relatively stable throughout this six-month period.

The changes in average P- and S-wave velocity experienced in this period, maximum of approximately +1.1 ms^{-1} and +0.3 ms^{-1} respectively, are smaller than the estimated uncertainties (2 ms^{-1}) and not significant. P- and S-wave amplitudes remain relatively stable, within 0.07 dB of the amplitude at the start of the reporting period, until 21st June 2009 when P- and S-wave amplitude drops by 0.11 db and 0.10 db respectively over 8 days (a relatively large change for the period). The average velocity changes across each of the five ray-path categories, defined according to their orientation with respect to the deposition hole and the in situ stress field, are small and similar for P- and S-waves.

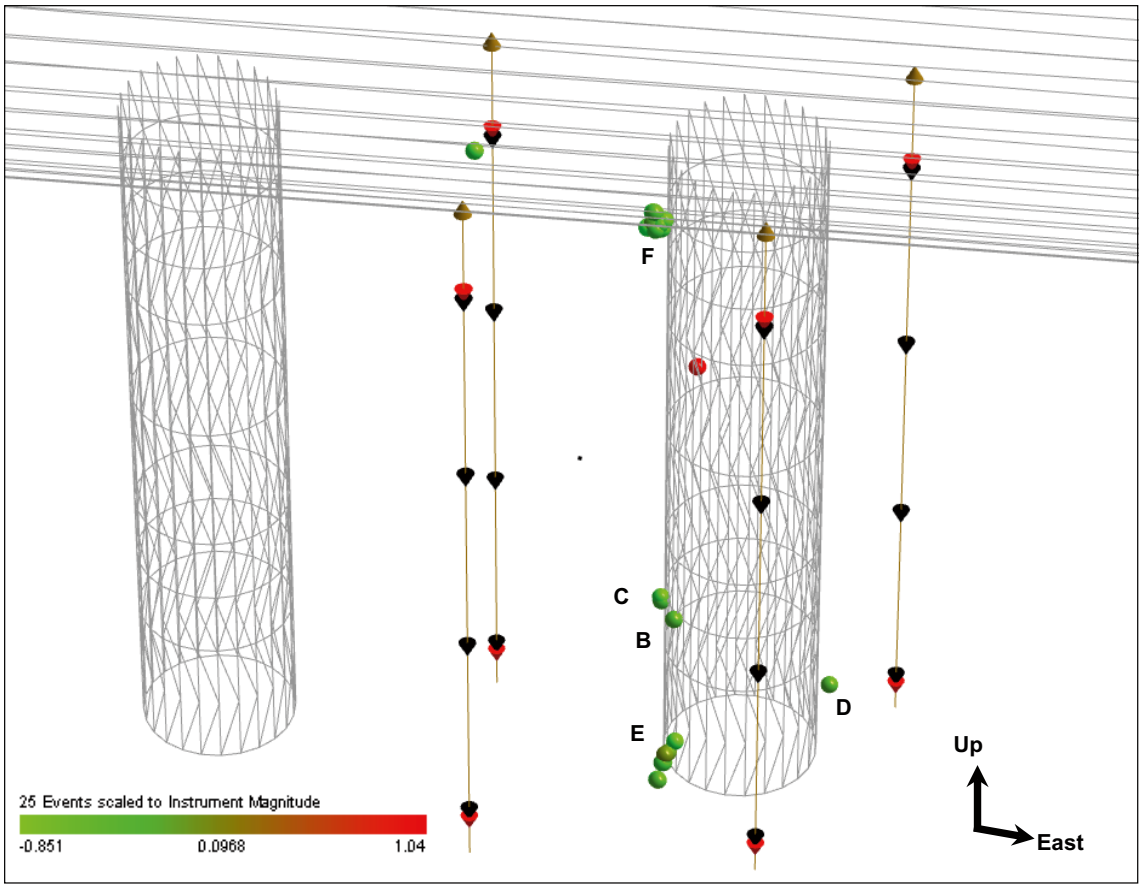

Figure ES-1. *Located AE events observed around the deposition hole for this monitoring period. Events are scaled to instrument magnitude. Labels B, C, D, E and F identify positions of clusters identified previously where events locate during this reporting period.*

Consequently, rock parameters show little variation for the same period. P- and S-wave amplitudes for the ray-path categories remain stable in April, May and June but a decrease in amplitude occurs for all ray-path categories between 21st June and 29th June. The trend for the rest of the monitoring period is for little change in amplitudes. Category S1 ray-paths, passing through a volume of high compressive stresses, exhibit the greatest variation. P- and S-wave velocity change and amplitude change from the start of monitoring (20th March 2003) are presented in Figure ES-2.

There are little changes in the environmental conditions in the tunnel and around the deposition hole, so the AE rates and small variations in velocity and amplitude observed are a reflection of these static conditions. With no short-term changes in temperature and pressure this report period is comparably stable.

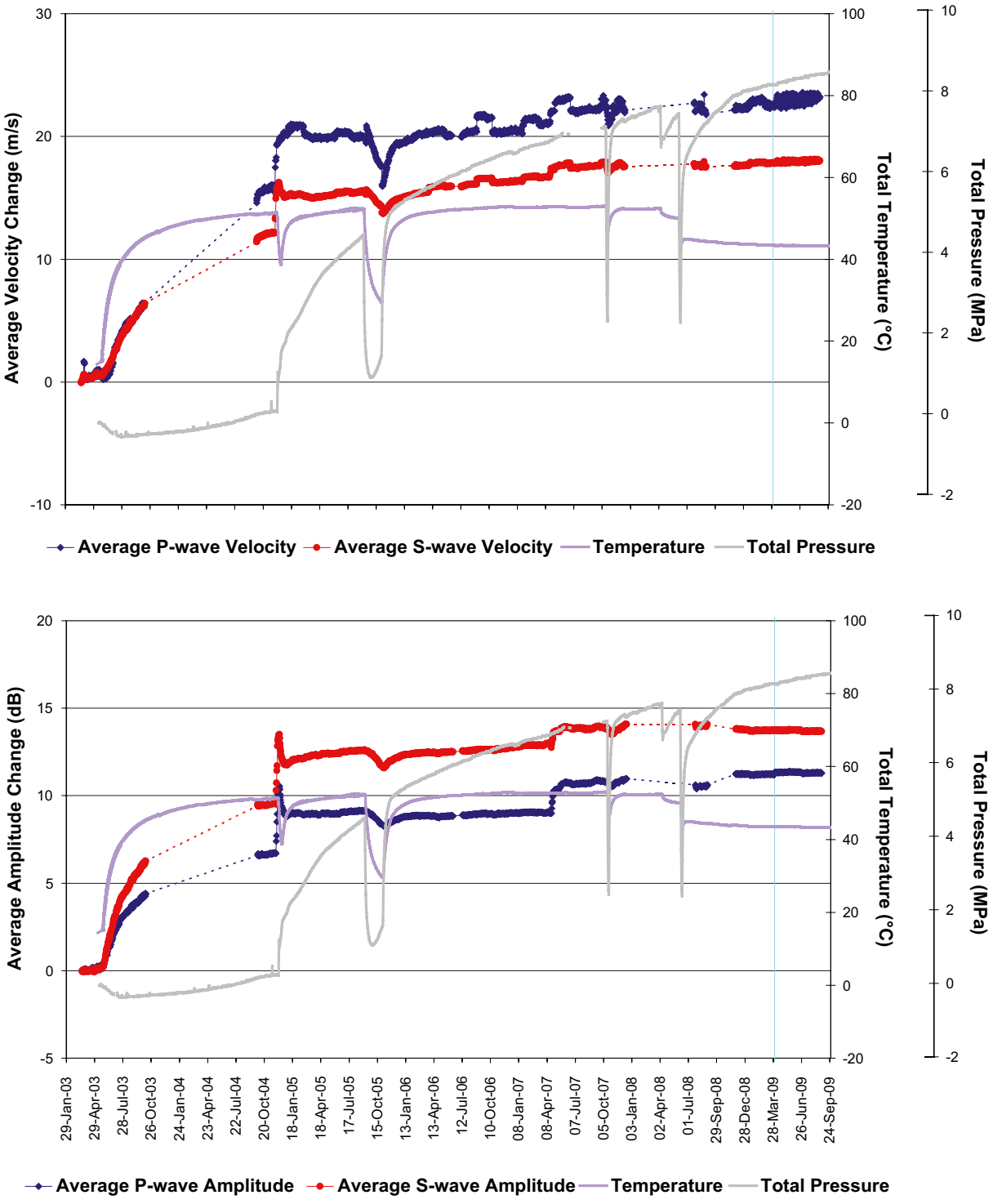

Figure ES-2. *Average velocity and amplitude changes since the start of the heating and pressurisation phase at the Prototype Repository. The vertical blue line indicates the start of the period analysed in this report (1st April 2009–30th September 2009).*

Contents

1 Introduction 9

2 Specific objectives 11

3 Results 13
3.1 Ultrasonic surveys 13
3.2 Acoustic emissions 22

4 Conclusions 35
4.1 Monitoring between April 2009 and September 2009 35
4.2 Summary of monitoring from the heating and pressurisation phase 36
4.3 Recommendations 37

References 51

Appendix 1 Previous monitoring at the prototype repository 53
Appendix 2 Methodology 55
Appendix 3 Processing parameters 63

1 Introduction

This report describes results from acoustic emission (AE) and ultrasonic monitoring around a canister deposition hole (DA3545G01) in the Prototype Repository Experiment at SKB's Hard Rock Laboratory (HRL), Sweden. The monitoring aims to examine changes in the rock mass caused by an experimental repository environment, in particular due to thermal stresses induced from canister heating and changes in pore pressures induced from tunnel sealing. Monitoring of this volume has previously been performed during excavation (Pettitt et al. 1999), and during stages of canister heating and tunnel pressurisation (Haycox and Pettitt 2005a, b, 2006a, b, Zolezzi et al. 2007, 2008, Duckworth et al. 2008, 2009, Haycox and Duckworth 2009). Further information on the previous monitoring undertaken can be found in Appendix 1. This report covers the period between 1st April 2009 and 30th September 2009 and is the ninth 6-monthly processing and interpretation of the results from the experiment.

The Prototype Repository Experiment (Figure 1-1) has been designed to simulate a disposal tunnel in a real deep repository for disposal of high-level radioactive waste. Its objective is 'to test and demonstrate the integrated function of the repository components under realistic conditions on a full scale and to compare results with models and assumptions'. The experiment consists of a 90 m-long, 5 m-diameter sub-horizontal tunnel excavated in dioritic granite using a Tunnel Boring Machine (TBM). The rock mass has two main discontinuous sets of sparse, en-echelon fractures (Patel et al. 1997). The Prototype Repository design incorporates six full-scale canister deposition holes which have been excavated vertically into the floor of the tunnel using a TBM converted to vertical boring. Each deposition hole measures 1.75 m in diameter and approximately 8.8 m in length. Simulated waste canisters, encased in a bentonite buffer, have been placed into each deposition hole and heated from within by specially designed electric heaters to simulate disposed radioactive material at elevated temperatures. The tunnel was then backfilled using a mixture of bentonite and crushed rock, and sealed using concrete plugs. A range of measurements are made in and around the tunnel and deposition holes.

AE and ultrasonic monitoring are tools for remotely examining the extent and severity of damage and disturbance around an excavation. Damage and disturbance can be induced by the excavation method itself, by the redistribution of stresses (loading or unloading) resulting from the void, or by environmental effects such as heating, saturation or pressurisation. Acoustic techniques are particularly adept

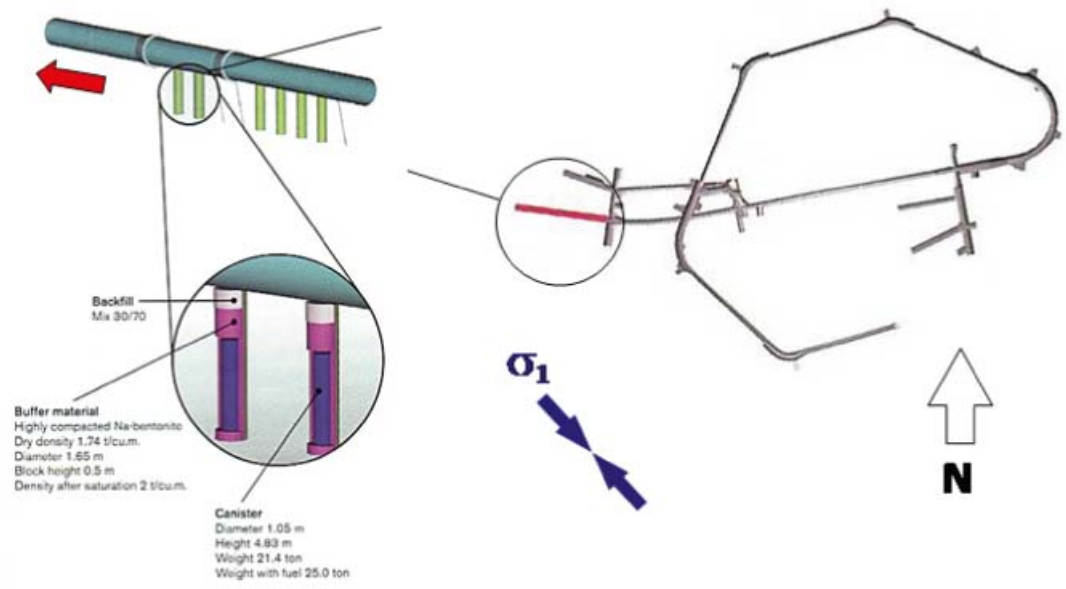

Figure 1-1. *Plan view of the experimental tunnels at the Äspö HRL and the location of the Prototype Repository. A schematic illustration of the final experimental set up is shown with canisters and bentonite clay buffer installed in the 1.75 m diameter deposition holes. Note the entrance of the tunnel is towards the left. Graphics are modified from SKB (1999).*

at assessing the Excavation Damaged or Disturbed Zone (EDZ) as they allow it to be mapped spatially and temporally with high resolution, and they allow the effect on the rock mass to be quantifiably measured. Furthermore, acoustic techniques allow investigations to be conducted remotely, without the need for potentially damaging coring. Young and Pettitt (2000) give a review of AE and ultrasonic results from a number of experiments conducted in different underground environments.

- AE monitoring is a 'passive' technique similar to earthquake monitoring but on a much smaller distance scale (source dimensions of millimetres). AEs occur on fractures in the rock when they are created or when they move. The data acquisition system triggers on AEs when they occur and records full-waveform information that can then be used to delineate the amount, time, location and mechanism of fracturing.
- Ultrasonic surveys are used to 'actively' examine the rock. In this case an array of transmitters sends signals to an array of receivers. Amplitude and velocity changes on the ray-paths can be interpreted in terms of changes in the material properties of the rock. Calculations using the velocities can determine changes in dynamic moduli, Young's modulus and Poisson's ratio, to give direct indications of the properties of the rock through which the ray-paths are directed. Crack density and saturation can also be calculated to determine changes in crack properties in the damaged and disturbed zones.

Appendix 2 provides detailed descriptions of the data acquisition and processing used during this and past monitoring periods. The ultrasonic array consists of twenty-four ultrasonic transducers configured as eight transmitters and sixteen receivers installed into four instrumentation boreholes using specially designed installation frames sealed within slightly expansive grout. The array is designed to provide good coverage for AE locations and provide 'skimming' ray-paths so as to sample the rock immediately adjacent to the wall of the deposition hole. ASC's InSite Seismic Processor (Pettitt and Young 2007), has been used to automatically process both the AE and ultrasonic survey data. The processing parameters used are shown in Appendix 3A and Appendix 3B. Data from daily ultrasonic surveys have been automatically picked and arrivals cross-correlated to a reference survey for high-precision measurements of P- and S-wave velocity changes throughout the experiment. Arrivals of AEs have been manually picked and three dimensional source locations have been calculated.

Between 28th August 2009 and the end of the reporting period, ultrasonic surveying was not possible from transmitters 2 to 8 (inclusive) due to an equipment malfunction. The malfunction was rectified on 4th November 2009 following onsite troubleshooting by SKB staff supervised remotely by an ASC engineer. AE triggering has been performed throughout the monitoring period. Figure 1-2 shows a time-line of when surveys and AE triggering occurs.

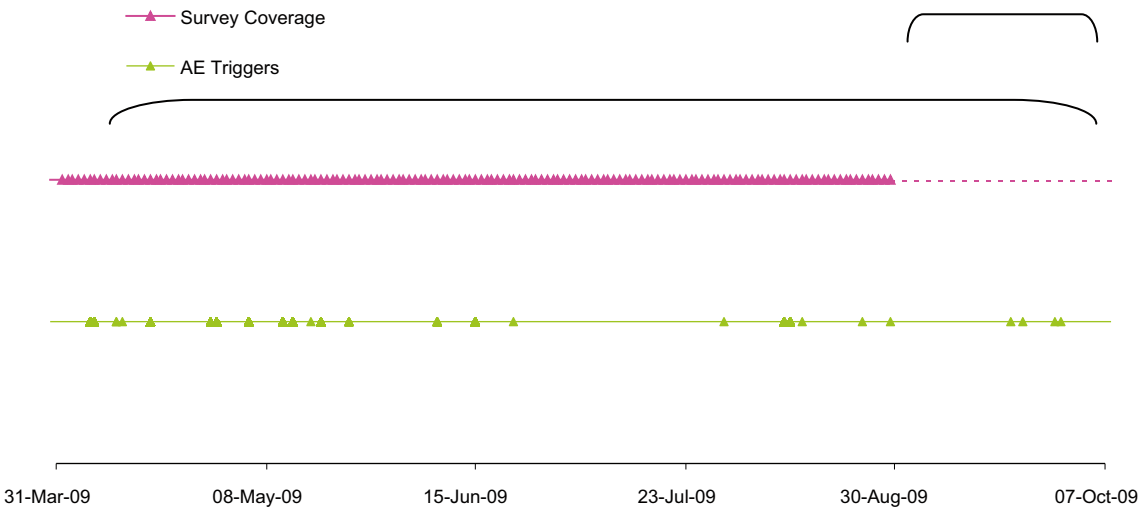

Figure 1-2. *Time-line showing the periods when the acquisition system was operational. Ultrasonic survey coverage was not available for transmitters 2 to 8 after 28th August 2009. The malfunction was rectified on 4th November 2009 after the end of the reporting period.*

2 Specific objectives

This six-month period of ultrasonic monitoring in the Prototype Repository Experiment has been undertaken with the following objectives:

- Produce accurate source locations for AEs so as to delineate the spatial and temporal extent of any brittle microcracking within the rock mass around the deposition hole and locate any movements on pre-existing macroscopic fractures.
- Conduct regular ultrasonic surveys to assess the effect of heating and other environmental changes on the velocity and amplitude of transmitted ultrasonic waves.
- Investigate changes in dynamic moduli and crack density to show how the properties of the rock volume around the deposition hole change throughout the experiment.
- Relate the AE and ultrasonic measurements to the measured *in situ* stress regime and other operating parameters such as temperature and fluid pressure.
- Outline how the results from this monitoring period relate to previous monitoring periods and to the overall experimental aims and objectives.

3 Results

3.1 Ultrasonic surveys

Environmental conditions in the tunnel and around the deposition holes can be ascertained from temperature and pressure measurements recorded by sensors embedded within the rock. The numerical data are supplied by SKB. During this reporting period, the temperature of the rock surrounding deposition hole DA3545G01 has been very stable, as shown in Figure 3-1. Eight sensors exhibit an increase of 0.1°C and five sensors exhibit an increase of 0.2°C over the six month reporting period (representing a 0.5% change). This follows the previous six months of stable temperature around the deposition hole in which a maximum decrease of 0.7°C was observed. The maximum temperature observed on the seven instruments during this reporting period is 45.3°C on TR6041. The minimum temperature observed is 30.7°C on TR6055. Temperature measurements are recorded to the nearest 0.1°C.

The pressure in the backfill above the deposition hole (Pore-Water Pressure) is shown in Figure 3-2a. Higher pressures are observed on all instruments between May and June 2009. The maximum pressure range recorded is 0.07 MPa for instrument UFA14 (representing a change of 7%). The maximum pressure observed on the seven instruments during this reporting period is 1.276 MPa on UFA14. The minimum pressure observed is 0.894 MPa on UFA15. Pore-water pressure measurements are recorded to the nearest 1 kPa.

Figure 3-2b is the total pressure in the rock adjacent to deposition hole. Both instruments exhibit a steady increase throughout the monitoring period. Pressure ranges from a minimum of 8.3 MPa to a maximum of 8.6 MPa at instrument PB616, and from a minimum of 4.9 MPa to a maximum of 5.7 MPa at instrument PB601. PB601 is located at the bottom of the deposition hole, whilst PB616 is located approximately half way up the deposition hole. Total pressure measurements are recorded to the nearest 1 kPa.

Velocity changes are measured between transmitter-receiver pairs by cross-correlating (CCR) data from the daily ultrasonic surveys. Using the cross-correlation procedure reduces uncertainty and allows a high-resolution analysis to be performed, with an estimated uncertainty of ± 2 ms^{-1} between surveys on individual ray-paths. Hence small changes in velocity can be observed. This is extremely important when changes in rock properties occur over only a small section (~5%) of the ray-path.

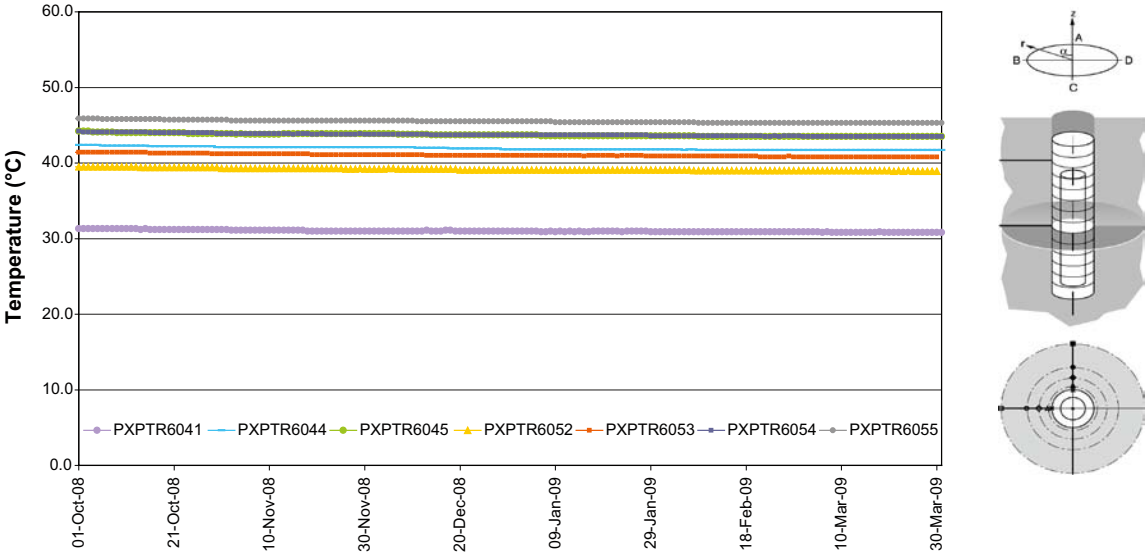

Figure 3-1. *Temperature of the rock mass around deposition hole DA3545G01 for the period between 1st April 2009 and 30th September 2009. The sensors are positioned mid-way up the deposition hole at different depths through the rock mass (see right-hand inset) (Goudarzi 2006).*

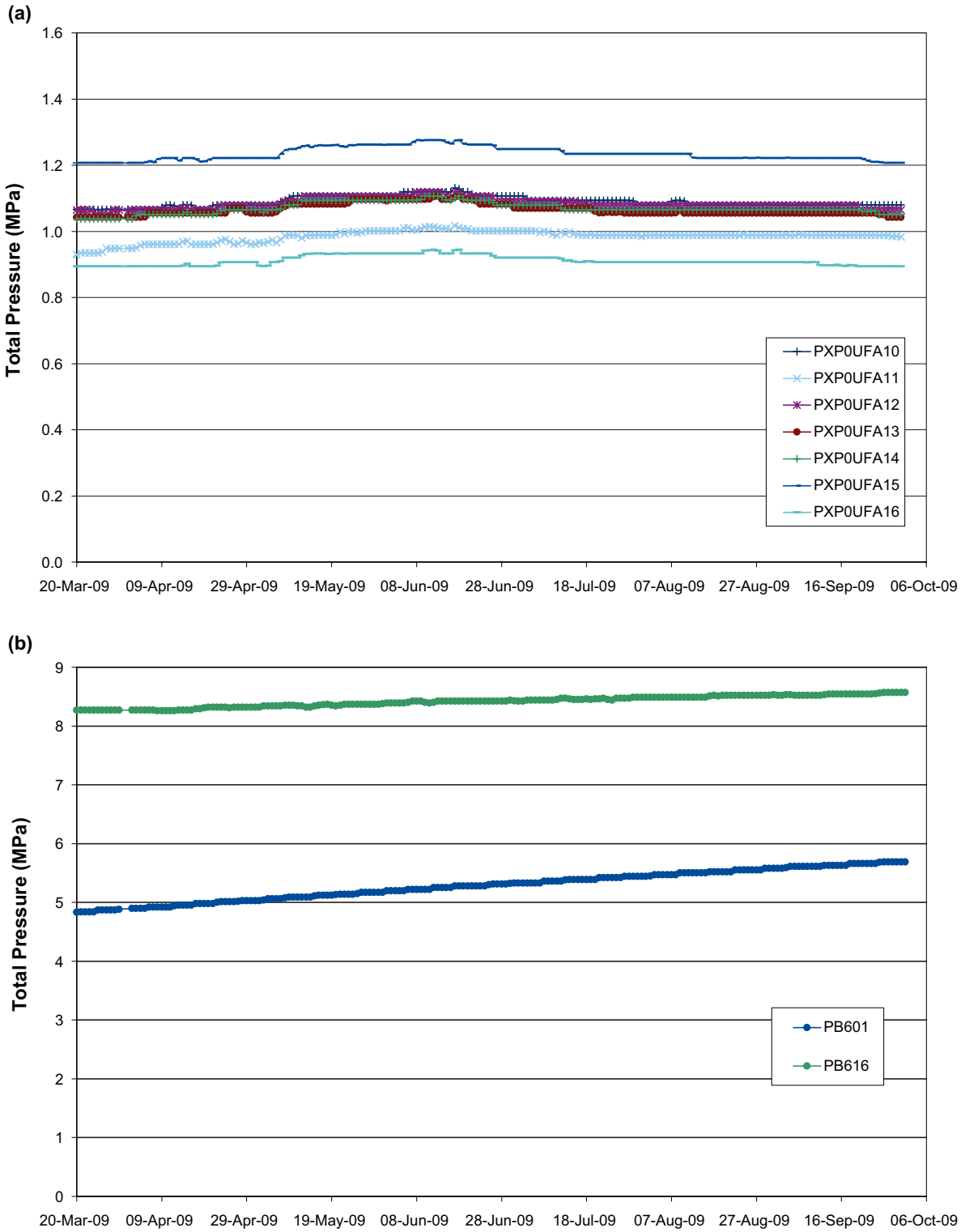

Figure 3-2. *Total pressure in (a) the backfill over deposition hole DA3545G01 and (b) the rock adjacent to deposition hole DA3545G01 for the period between 1st April 2009 and 30th September 2009.*

A new reference survey was used for processing data in the previous six-month reporting period (Haycox and Pettitt 2009a) when refurbishment and reinstallation of the equipment led to a change in characteristics of waveforms. The new survey, performed on 28th November 2008, is used as the reference survey for cross-correlating the data in this report.

Figure 3-3 shows the three-dimensional velocity structure for the reference survey recorded on 28th November 2008. A total of 79 ray-paths are processed for P-wave velocity and 49 for S-wave velocity. The structure is principally isotropic but with some heterogeneities. These could be a combination of measurement uncertainty (estimated at ± 30 ms^{-1} for absolute velocity measurements) and localised effects from the deposition hole and stress field.

Ultrasonic surveying was not possible for transmitters 2 to 8 (inclusive) between 28th August 2009 and the end of the reporting period due to equipment malfunction. The malfunction was fixed on 4th November 2009. Consequently, measurements in the change of amplitude, velocity and rock properties are affected after 29th August 2009 as smaller numbers of ray-paths are used in the calculations, and certain ray-path categories, defined by Pettitt et al. (1999), no longer have data. As transmitter 1 was active throughout the monitoring period, average velocity change and amplitude change plots are possible for the whole period (Figure 3-4). The maximum magnitude of velocity change is 2.1 ms^{-1} for P-waves and 0.6 ms^{-1} for S-waves. The P-wave amplitudes increase from 15th May 2009 and reach a maximum of 0.13 dB higher by 24th August 2009. S-wave amplitudes do not vary by more than 0.05 dB until 19th June 2009, when amplitudes decrease by 0.12 dB over the following 13 days. The amplitudes remain relatively stable until 29th August 2009. There is a steep decrease in amplitudes between 29th and 30th August 2009 when P- and S-wave amplitudes decrease by 0.07 and 0.13 dB respectively. This coincides with the date of the equipment malfunction on transmitters 2 to 8 and is probably related to how the pulser-box operates following the loss of the other transmitters.

Average P- and S-wave velocity changes for ray-paths involving all transmitters for the period until 28th August 2009 are shown in Figure 3-5a. The maximum change in average velocity is approximately +1.1 ms^{-1} for P-waves and approximately +0.3 ms^{-1} for S-waves, with average changes in the region of 0.5 ms^{-1} for P-waves and 0.1 ms^{-1} for S-waves. The changes in average velocity experienced in this period are therefore smaller than the estimated uncertainties (2 ms^{-1}) and not significant. The P-wave velocity varies between days up to 1.2 ms^{-1} and is particularly apparent between April and July 2009. This is due to the cumulative effect of individual sample point changes on ray-paths. Overall, the magnitude of the average velocity changes throughout this monitoring period is small and significantly smaller than the velocity resolution of 2 ms^{-1} estimated for ultrasonic measurements. However, changes on individual ray-paths are more pronounced. During this monitoring period 19 out of the 79 ray-paths show a magnitude change in P-wave velocity, measured against the survey on 28th November, greater than 2 ms^{-1}. The maximum change observed is an 6.1 ms^{-1} increase on ray-path 5–16 in the 'Far' category. There is no spatial pattern in which ray-paths exhibit a greater than 2 ms^{-1} change. No ray-paths show an absolute change in S-wave velocity greater than 1 ms^{-1}. P- and S-wave amplitudes remain relatively stable, within 0.07 dB of the amplitude at the start of the reporting period, until 21st June 2009 (Figure 3-5b). Over the next 8 days P- and S-wave amplitude drops by 0.11 db and 0.10 db respectively. The amplitudes generally remain lower than at the start of the monitoring period until 29th August 2009. There is no overall trend evident in P- or S-wave amplitudes during this period. The small changes in average velocity and amplitude may reflect the stable environmental (i.e. temperature and pressure) conditions in and around the canister deposition hole.

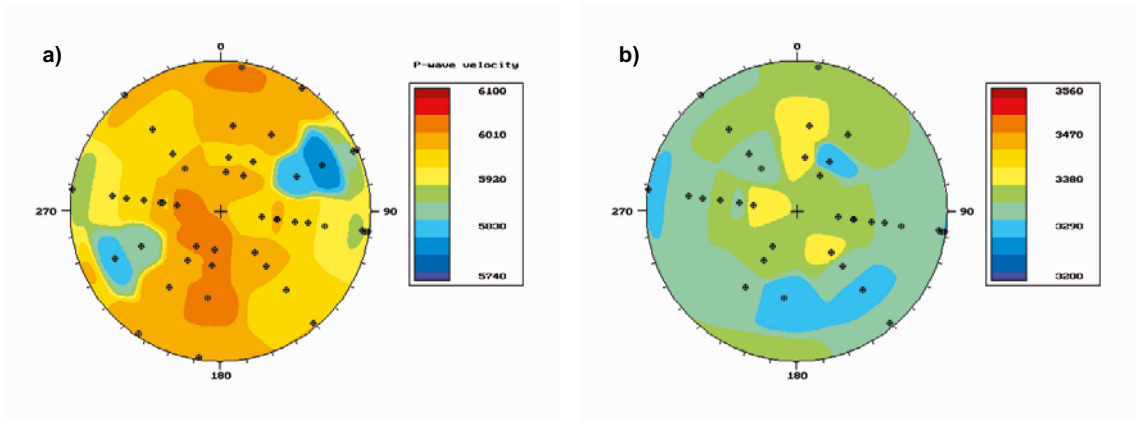

Figure 3-3. *Lower hemisphere stereonets of a) P-wave velocity and b) S-wave velocity for the reference survey on 28th November 2008. The ray path orientations are shown by black markers.*

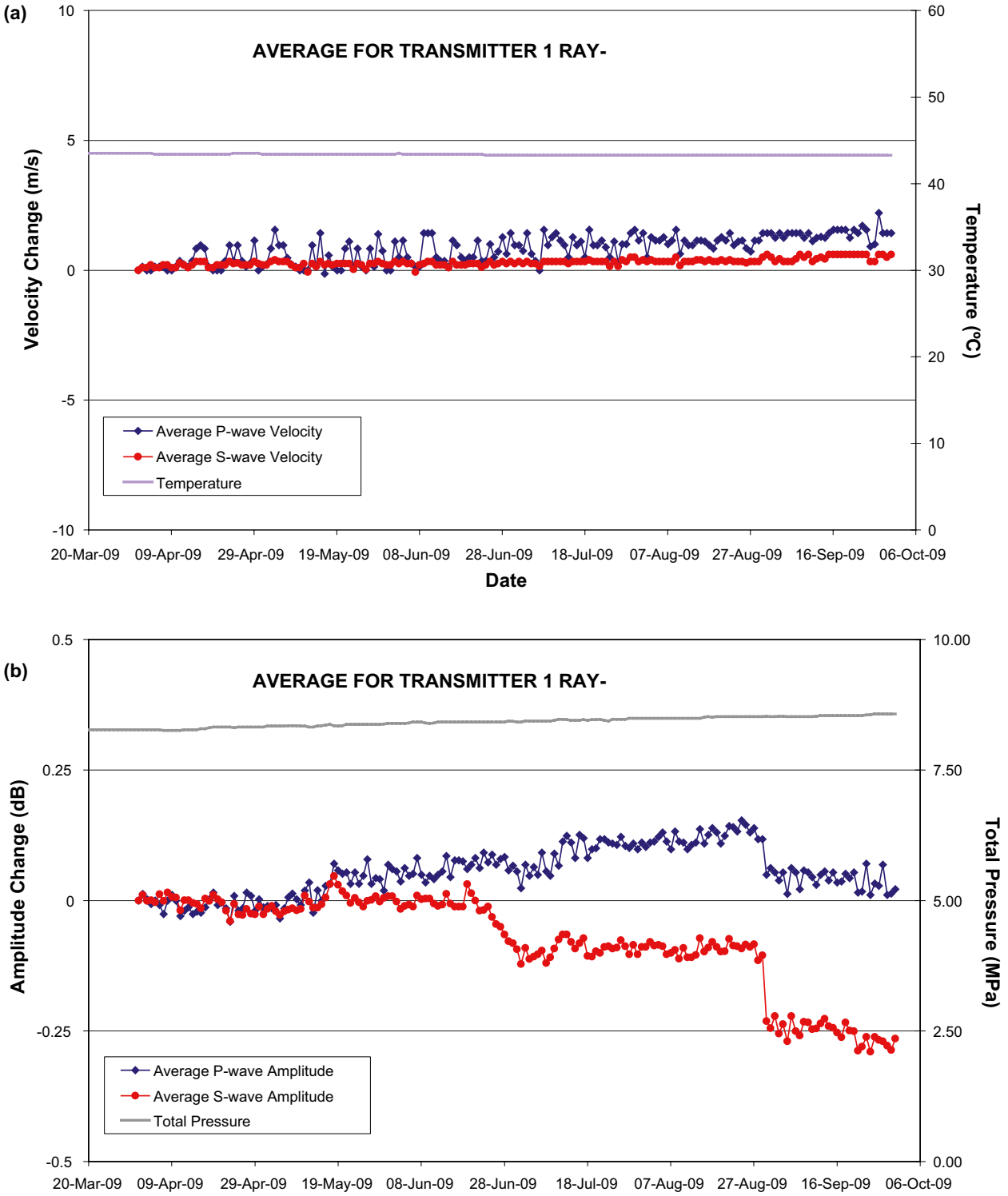

Figure 3-4. *Average P- and S-wave (a) velocity change (ms^{-1}) and (b) amplitude changes (dB) for transmitter 1 ray-paths. Temperature of the surrounding rock mass (TR6045) and total pressure in the backfill (UFA15) are displayed on the secondary axes.*

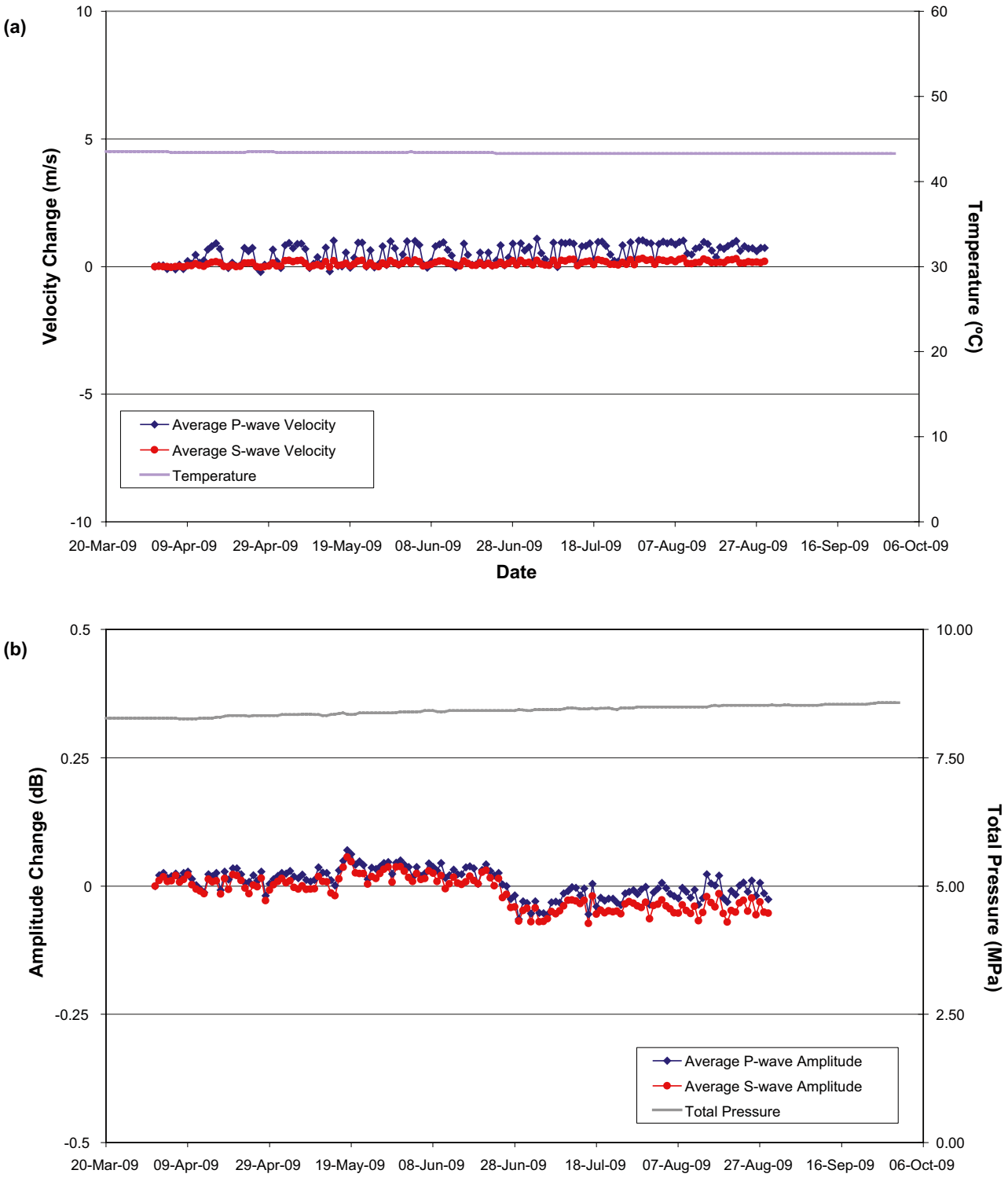

Figure 3-5. *Average P- and S-wave (a) velocity change (ms^{-1}) and (b) amplitude changes (dB). Temperature of the surrounding rock mass (TR6045) and total pressure in the backfill (UFA15) are displayed on the secondary axes.*

Pettitt et al. (1999) categorised ray-paths from ultrasonic surveys into six types depending on their orientation with respect to the deposition hole and the in situ stress field (Figure 3-6). Ultrasonic results are interpreted in terms of the disturbed and damaged regions around the void during the excavation phase of the experiment. Pettitt et al. (2000) undertook three-dimensional elastic stress modelling to describe these zones of stress.

Velocity changes recorded along selected transmitter-receiver paths relating to ray-paths of the S3 category are shown in Figure 3-7. Category S3 ray-paths pass within centimetres of the deposition hole through the excavation damaged zone, in a region of low compressive or tensile stress. These particular ray-paths have been chosen because they provide a comparison of velocity changes along the length of the deposition hole. Each plot is accompanied by a schematic diagram showing a perspective of the region through which the ray-path passes and also the transmitter-receiver configuration. In general, little variation is observed in P- or S-wave velocity change during this monitoring period, with the majority of surveys experiencing no change or one sample-point change (2 ms^{-1}) from the 1st April 2009. Figure 3-8 shows velocity changes recorded along selected ray-paths of the S1 category. These ray-paths pass through a region of compressive stress and permanent damage close to the wall of the deposition hole and are imaged by relatively high AE activity during periods of excavation. Velocity changes experienced on this ray-path are similar to S3 category ray-paths, in which minor changes (< 2 ms^{-1}) are observed in P-wave velocity and with very little change observed in S-wave velocity. The changes experienced are of the order of the estimated uncertainties and therefore not deemed to be significant.

In Figure 3-9, the average velocity changes across each of the ray-path categories described in Figure 3-6 have been compared in order to analyse small and consistent changes in the recorded measurements. Although there are changes in velocity between days, the maximum change from the measurement at the start of the reporting period is 1.7 ms^{-1} for the Far category ray-path. S-waves exhibit less variation with category C1 ray-paths showing a maximum change of 0.4 ms^{-1}. P-wave velocity changes have been greater than S-wave velocity changes in previous reporting periods (e.g. Duckworth et al. 2008, 2009); the measurements in Figure 3-9 continue this trend.

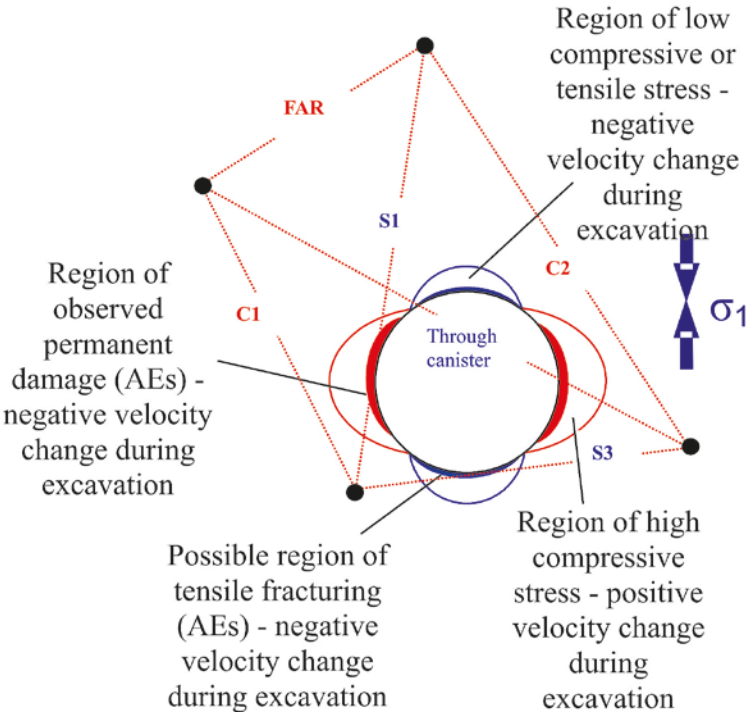

Figure 3-6. *Interpretation of the ultrasonic results during excavation in terms of disturbed and damaged regions around the deposition hole. Zones of induced stress are inferred from elastic modelling and the* σ_1 *orientation, after Pettitt et al. (1999).*

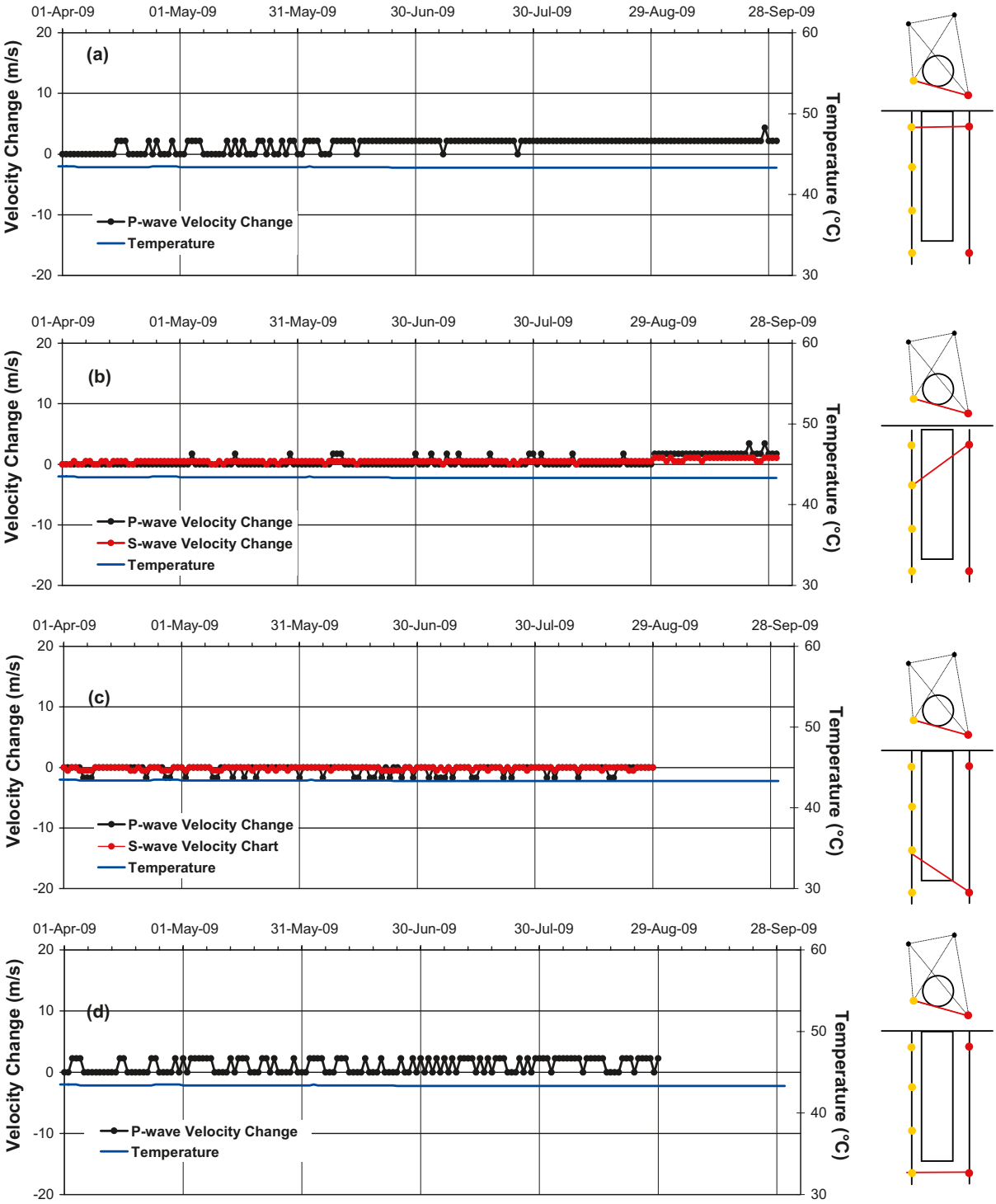

Figure 3-7. *Velocity changes measured on ray-path category S3 (Figure 3-6) for deposition hole DA3545G01. Ray-paths shown are from transmitter (t_n) to receiver (r_n) for (a) t_n=1, r_n=5; (b) t_n=1, r_n=6; (c) t_n=2, r_n=7 and (d) t_n=2, r_n=8. Schematic diagrams on the right indicate the relative positions of transmitter (red) and receiver (gold). Temperature (TR6045, blue line) is displayed on the secondary axes.*

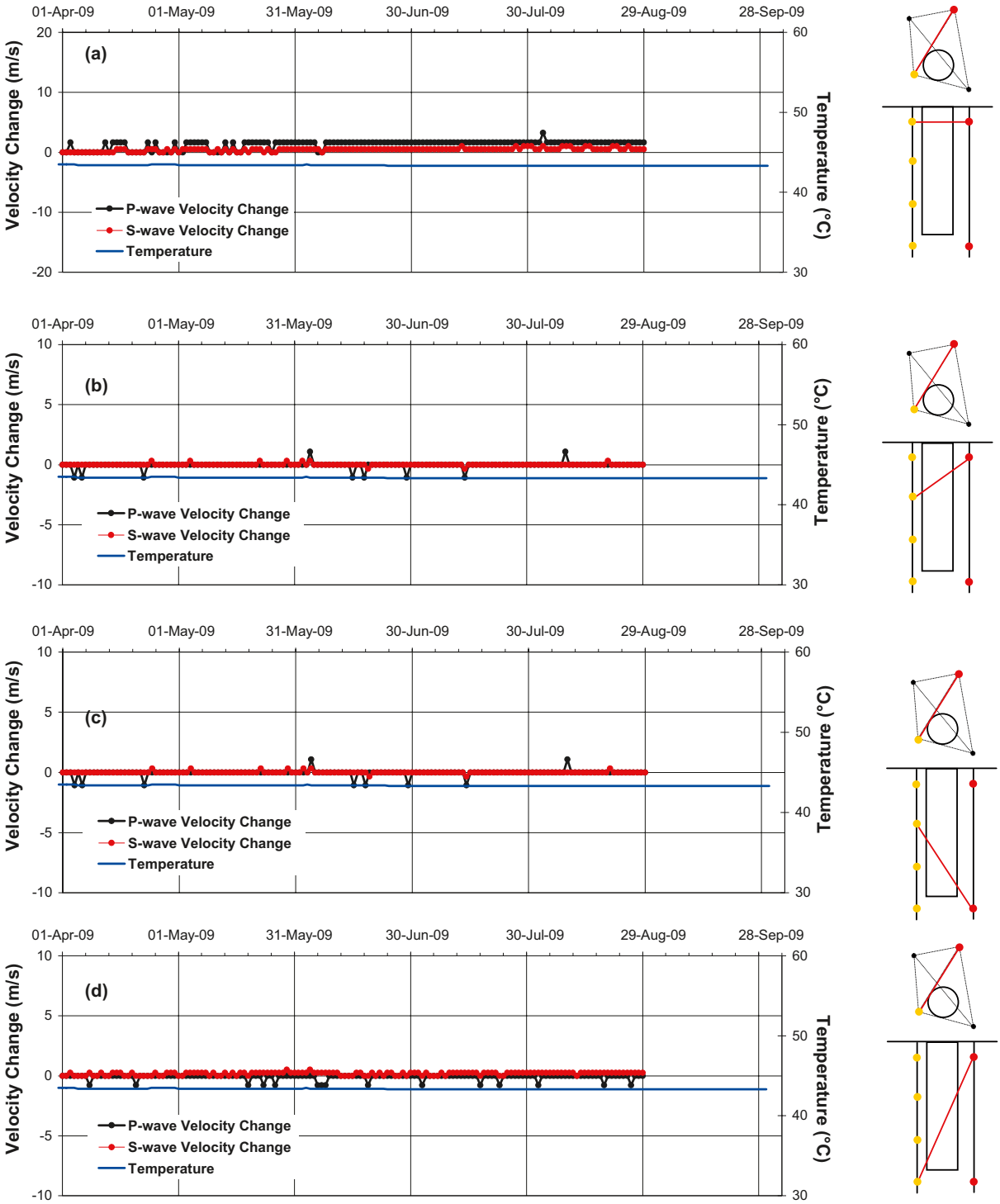

Figure 3-8. *Velocity changes measured on ray-path category S1 (Figure 3-6) for deposition hole DA3545G01. Ray-paths shown are from transmitter (t_n) to receiver (r_n) for (a) t_n=7, r_n=5; (b) t_n=7, r_n=6; (c) t_n=8, r_n=6 and (d) t_n=7, r_n=8. Schematic diagrams on the right indicate the relative positions of transmitter (red) and receiver (gold). Temperature (TR6045, blue line) is displayed on the secondary axes.*

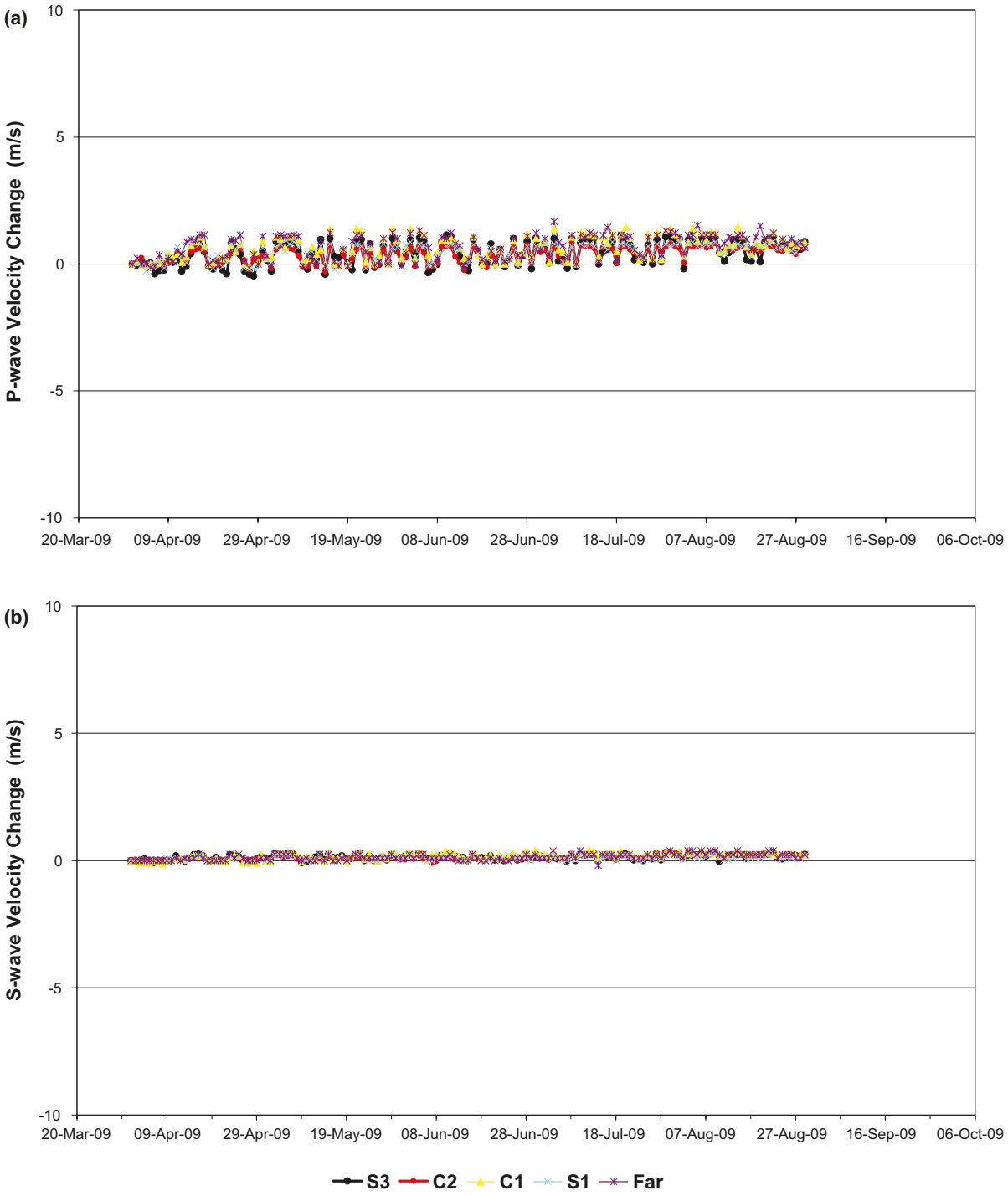

Figure 3-9. *Average velocity changes for the five category ray-paths (S1, S3, C1, C2, Far) around deposition hole DA3545G01 for (a) P-waves and (b) S-waves.*

The average amplitude changes across the five category ray-paths are shown in Figure 3-10. In April, May and June 2009, P-wave amplitudes (Figure 3-10a) for four ray-path categories remain stable but C1 ray-paths exhibit a slight increase reaching 0.17 dB higher by 30th May 2009. A decrease in amplitude occurs for all ray-path categories between 21st June and 29th June. The trend for the rest of the monitoring period is for little change in amplitudes. A similar pattern is observed for S-wave amplitudes in Figure 3-10b, other than on categories other than C1 and S3 where consistent increases of 0.17 and 0.11 dB respectively are observed after 29th June.

Figure 3-11 shows the changes in rock properties calculated using average velocities and amplitudes for the five category ray-paths. Young's Modulus (Figure 3-11a) describes the stiffness of the rock mass, Poisson's Ratio (Figure 3-11b) is the ratio of latitudinal to longitudinal strain, Crack Density (Figure 3-11c) is a measure of the extent of fracturing per unit volume and Saturation (Figure 3-11d) relates to the number of cracks per unit volume containing fluids. Crack Density and Saturation of the rock mass are determined using the method of Zimmerman and King (1985), as described in Appendix 2.

All rock parameters in Figure 3-11 show little variation between 1st April and 29th August 2009. Young's Modulus shows a maximum change of 0.2×10^{8} Pa, Poisson's ratio shows a maximum change of 7×10^{-5}, Crack Density shows a maximum change of -1.1×10^{-4}, and Saturation shows a maximum change of -7.8×10^{-4}.

There is little change in the environmental conditions in the tunnel and around the deposition hole, so the small variations in velocity and amplitude observed are a reflection of these static conditions. With no short-term changes in temperature and pressure this report period is comparatively stable relative to short-term variations observed in previous monitoring periods.

3.2 Acoustic emissions

The AE monitoring has been successfully conducted for all six months of this monitoring period. The parameters used to process AEs are shown for reference in Appendix 3. A trigger is described as an event that has been acquired by the monitoring system, but may not be of sufficient energy or 'quality' to be located during the processing procedure. Noisy events, those that appear masked by electrical, environmental, or man-made noise, have been removed from the dataset allowing a more accurate representation of the fracturing occurring within the rock. There were a total of 2,881 triggers during this reporting period. The triggers have been manually inspected to determine their origin. The majority of the triggers are large amplitude, low frequency events that have first arrivals on the upper sensors suggesting they were caused by noise from tunnels adjacent to the prototype. 30 events have been identified, of which 25 located successfully in the region where the array coverage is good. The estimated uncertainty for the locations of these events around the deposition hole is less than 5 cm, determined using calibration 'hits' performed within the deposition holes after excavation (see Appendix 2 for further details).

The temporal distribution of the 25 AE events is shown in Figure 3-12. A peak in activity occurs on 8th June 2009, when 19 events are located in a single day. The average number of located AEs per day is 0.14. This is greater than the previous six-month period, but is still a historically low activity rate for the Prototype Repository (see Table 3-1). If the events on 8th June are not included, the average event rate is 0.03 AEs per day. The low AE activity signifies very little damage or disturbance around the repository.

Figure 3-13 shows the locations of AEs relative to the physical features of the Prototype Repository. Instrumentation boreholes are represented by the brown vertical lines, and the tunnel and deposition hole are represented by the grey wireframe structures. 24 of the events locate very close to deposition hole DA3545G01. The remaining event locates between the two deposition holes directly underneath the tunnel. Example waveforms, recorded on different channels, from clusters near the bottom of the deposition hole are shown in Figure 3-14. Figure 3-15 has example waveforms from events that locate towards the top of the deposition hole. The waveforms demonstrate the high quality data that are recorded using the array.

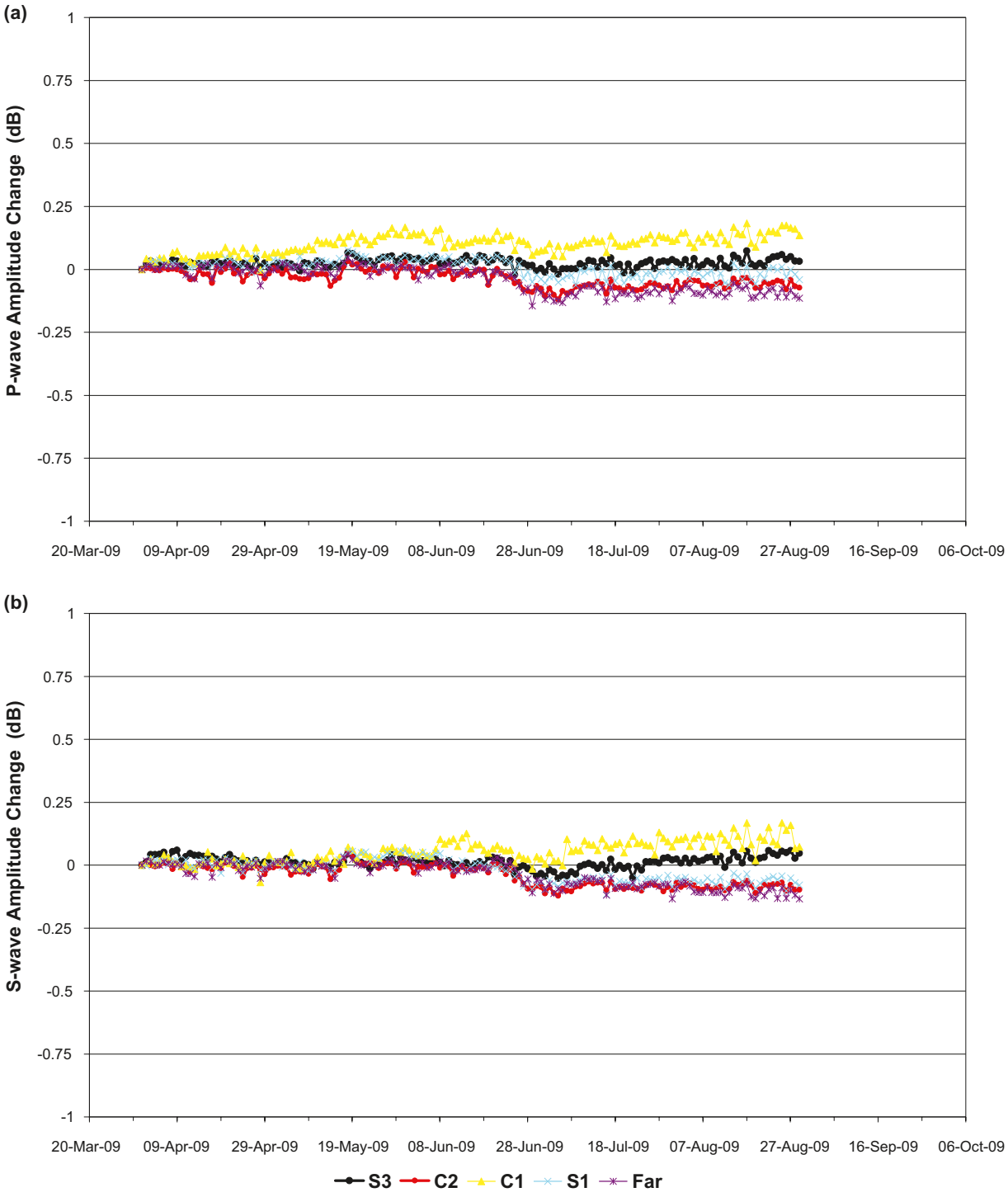

Figure 3-10. *Average amplitude changes for the five category ray-paths (S1, S3, C1, C2, Far) around deposition hole DA3545G01 during this report period for (a) P-waves and (b) S-waves.*

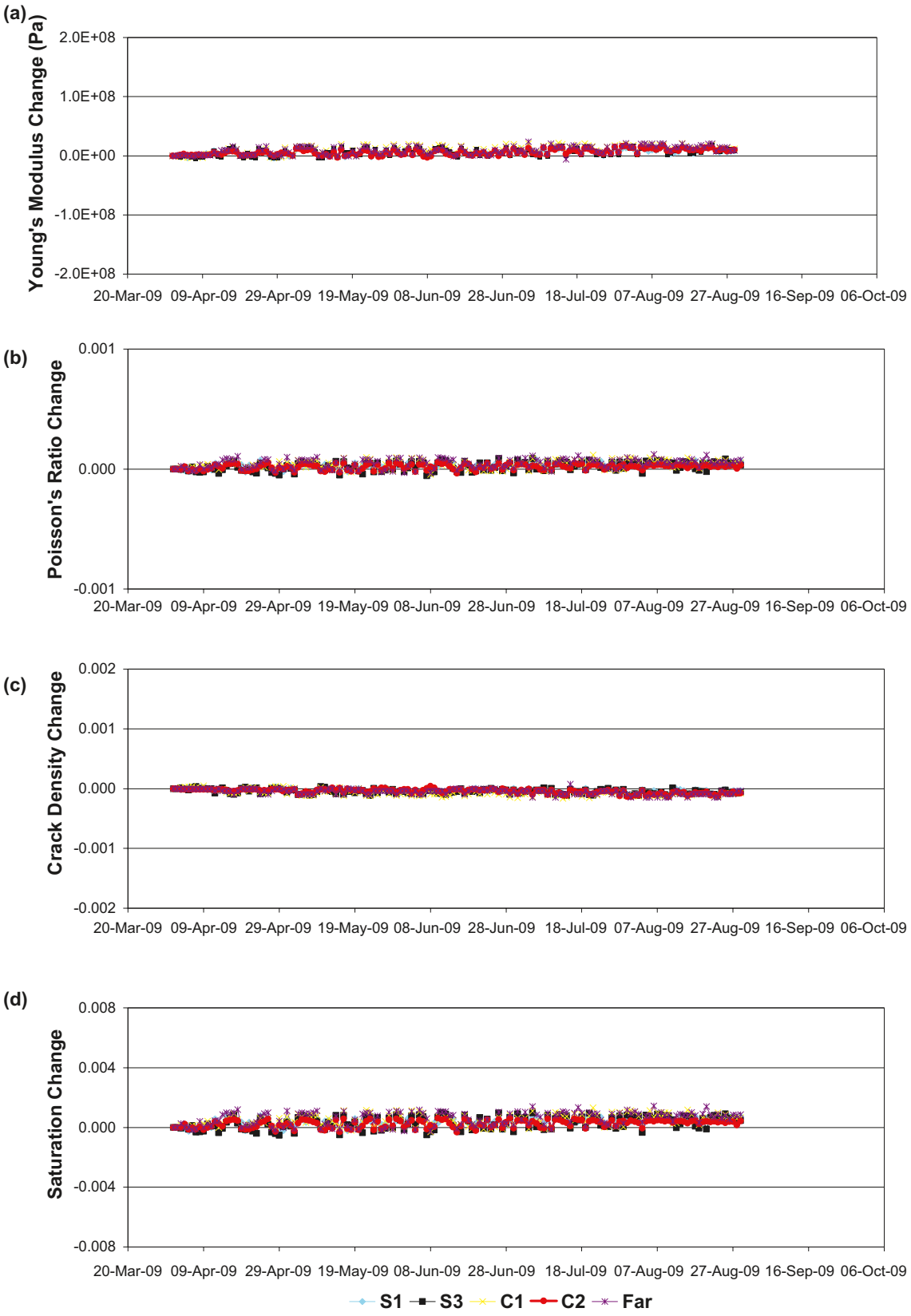

Figure 3-11. *Changes in rock parameters, calculated using average P- and S-wave velocities and amplitudes, for the five ray-path categories for (a) Young's Modulus, (b) Poisson's Ratio, (c) Crack Density and (d) Saturation.*

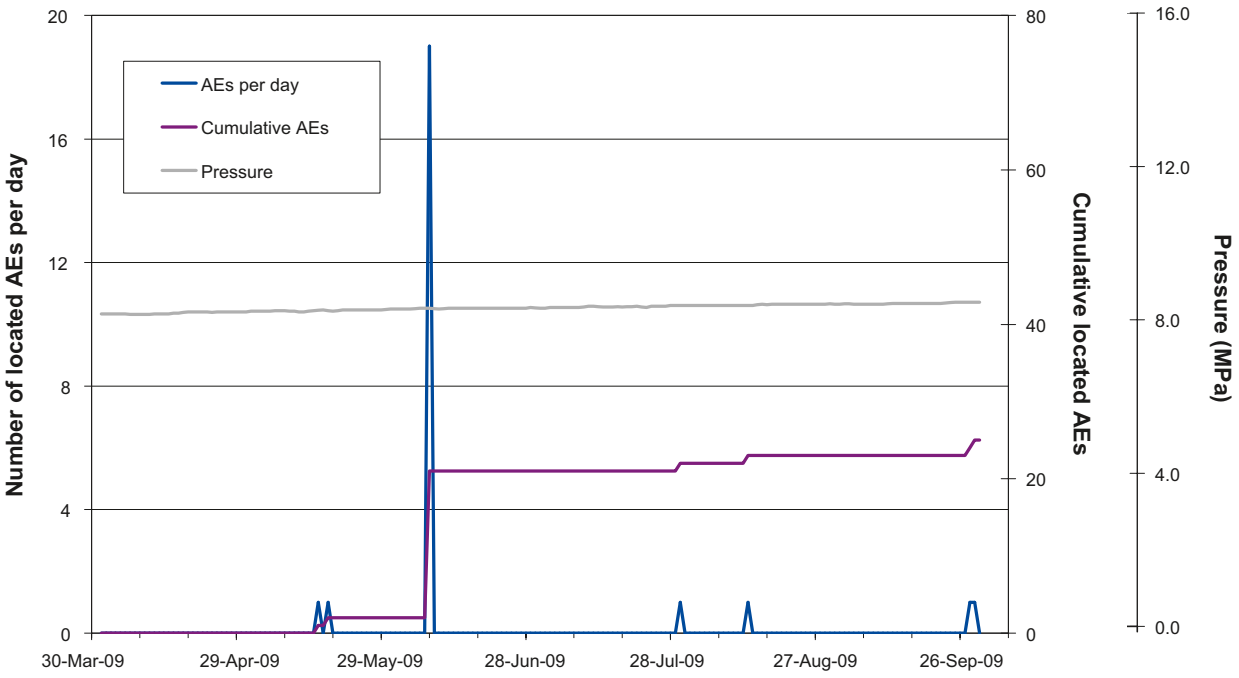

Figure 3-12. *Temporal distribution of the 25 AEs observed during this report period. The number of events per day is shown on the left axis and indicated by the blue line, and cumulative number of AE events is shown on the right-hand axis and indicated by the purple line. Also shown is the pore-water pressure (measured on instrument PB616) in the tunnel backfill over the deposition hole.*

Table 3-1. Average daily number of located AEs for the six monthly report periods starting 1st October 2004 and finishing with the end of this report period on 30th September 2009.

Time Period	Average Number of Events per Day
1st October 2004 to 31st March 2005	0.32
1st April 2005 to 30th September 2005	0.21
1st October 2005 to 31st March 2006	0.27
1st April 2006 to 30th September 2006	0.80
1st October 2006 to 31st March 2007	0.40
1st April 2007 to 30th September 2007	0.63
1st October 2007 to 31st March 2008	0.90
1st April 2008 to 30th September 2008	0.38
1st October 2008 to 31st March 2009	0.09
1st April 2009 to 30th September 2009	0.14

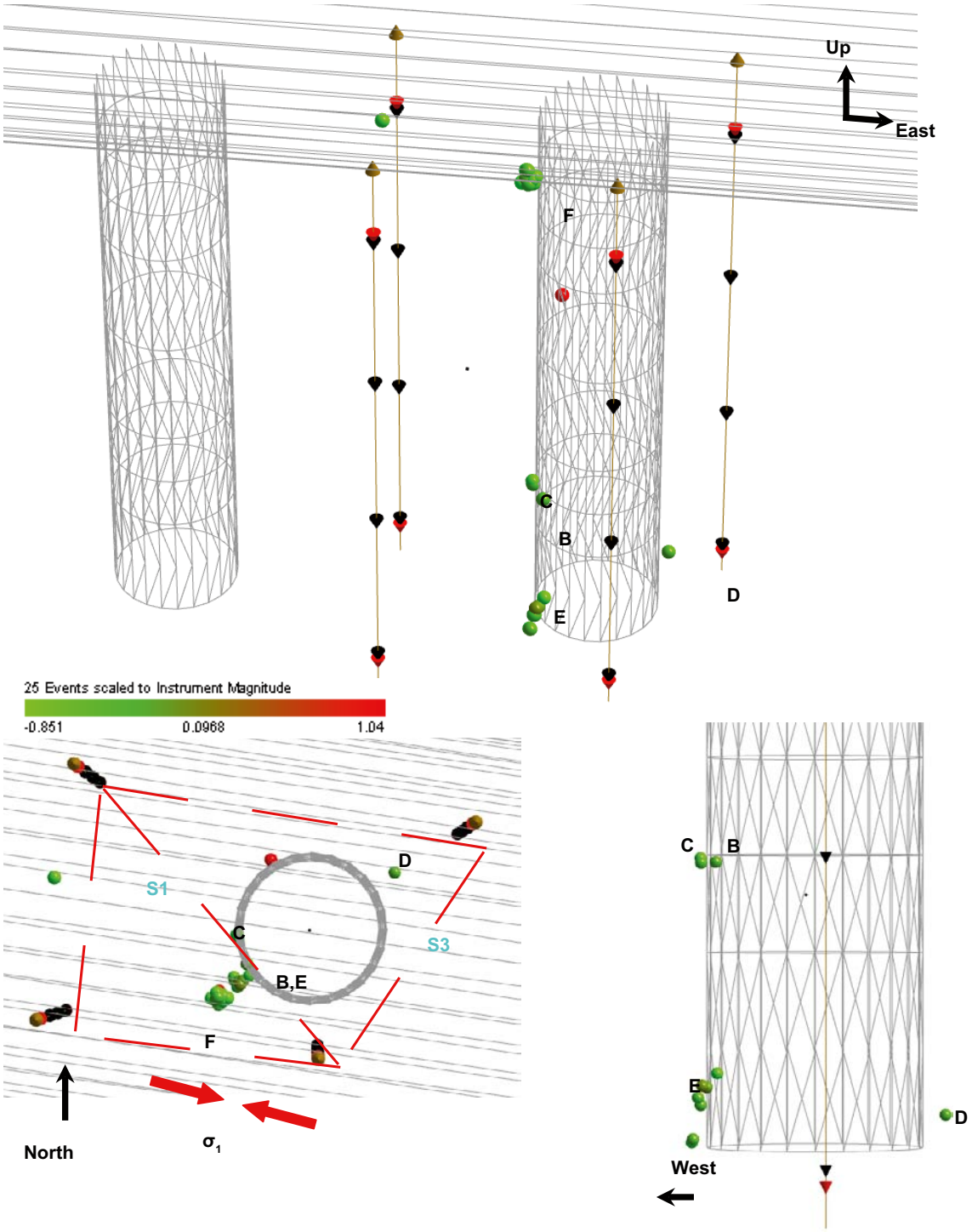

Figure 3-13. *Three views showing the clustered AE activity located around deposition hole DA3545G01. (Top: Oblique view looking north; Bottom left: Plan view with the five category ray-paths used in the ultrasonic survey shown relative to the deposition hole; Bottom right: Close-up view of the deposition hole.) Events are scaled to instrument magnitude (coloured bar, inset).*

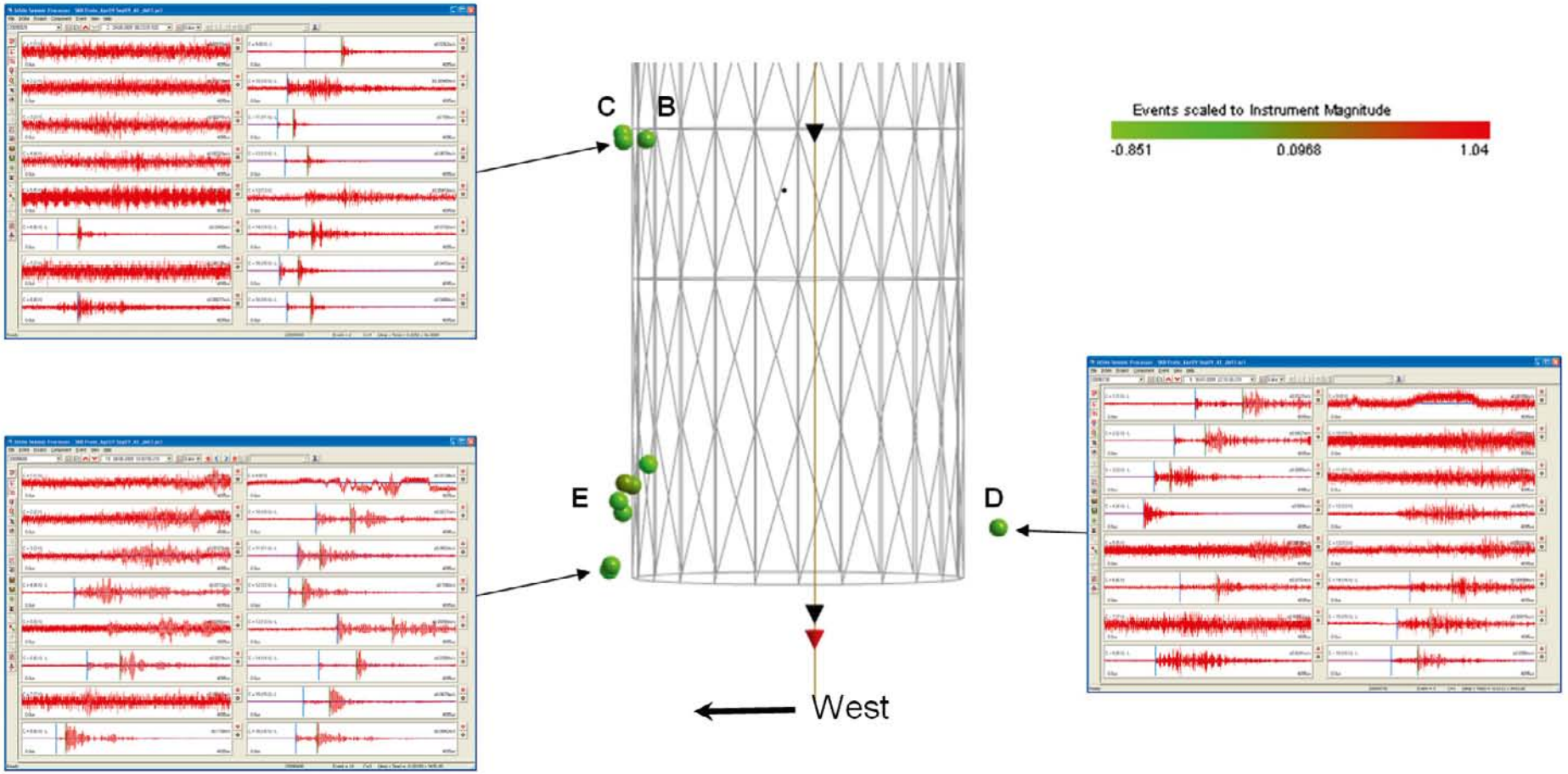

Figure 3-14. *Waveforms for selected events from three clusters shown in relation to a transverse view of AE activity. Events are scaled to instrument magnitude (coloured bar, inset).*

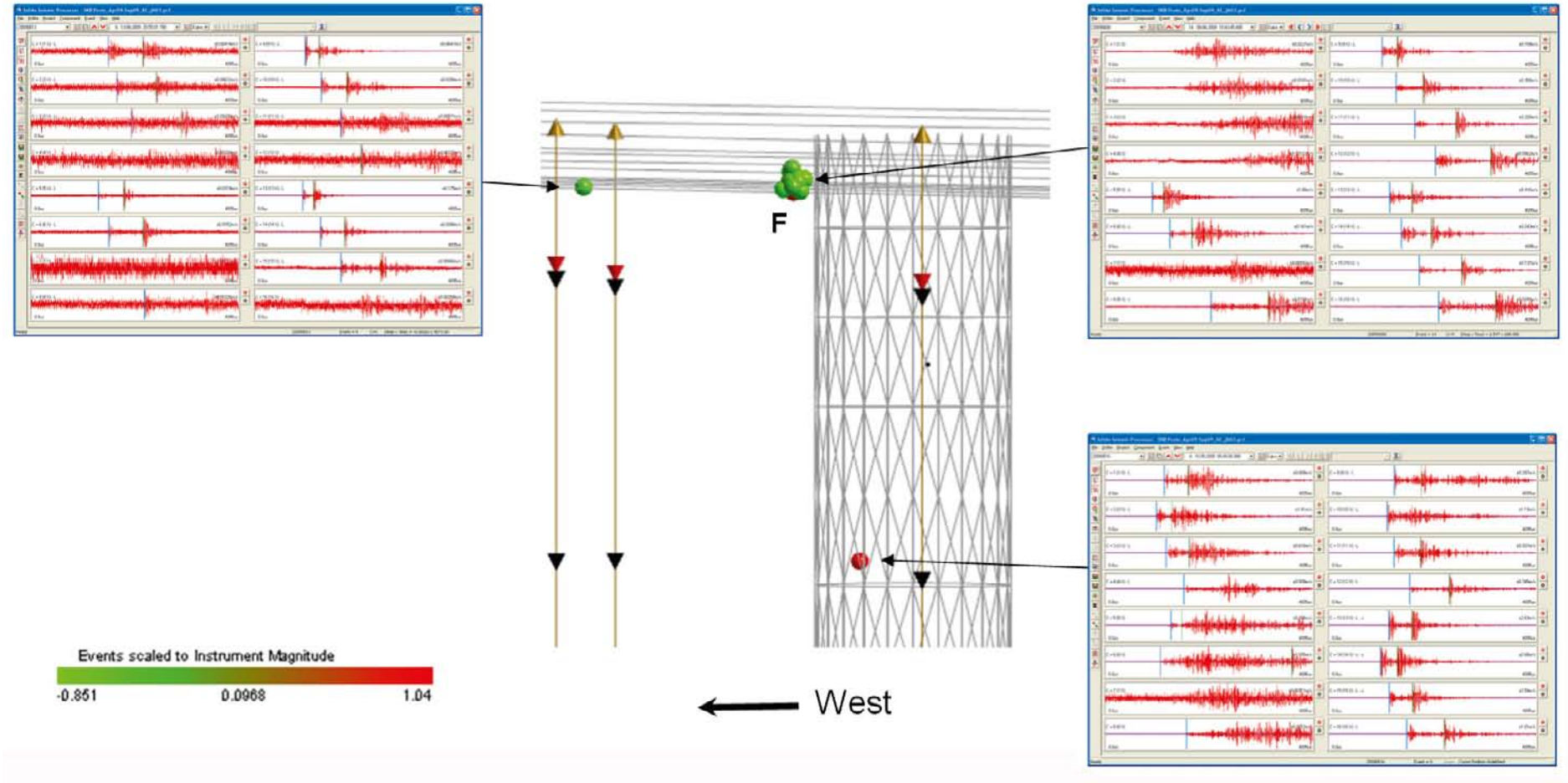

Figure 3-15. *Waveforms for selected events shown in relation to a transverse view of AE activity. Events are scaled to instrument magnitude (coloured bar, inset).*

In previous monitoring periods, events have been observed to cluster in specific locations designated A, B, C, D and T. During this period, no events are observed to locate in Cluster A or T. Cluster B consists of a single AE event in this period at N, E, D = (269.09, 919.70, 455.07). The event is located on the south west side of deposition hole DA3545G01. This cluster was observed in previous monitoring periods by Duckworth et al. (2008, 2009), and Haycox and Pettitt (2009a). The cluster occurs in a volume associated with the S1 ray-path category which passes through a region characterised by high compressive stress.

Two events locate at Cluster C with a centre located at approximately N, E, D = (269.44, 919.58, 455.06) (Table 3-2). This cluster is at a similar depth to Cluster B but further to the west side of the deposition hole, first classified by Duckworth et al. (2008).

One event locates at the position of Cluster D during this period at N, E, D = (270.25, 921.58, 457.17). Cluster D occurs in the high compressive stress region diametrically opposite to Clusters B and C during excavation (Figure 3-14). Events have been located at this position during the previous three monitoring periods having first been identified by Duckworth et al. (2008).

Two new clusters, where significant activity has not been observed since deposition hole excavation, exhibit activity during this reporting period and are defined as E and F in Figure 3-13. The cluster of seven events at position E is located towards the bottom, and the south west side, of the deposition hole. The events have average location N, E, D = (268.87, 919.59, 457.03), although they are not as tightly clustered, particular in depth. Cluster F consists of 13 events with average location N, E, D = (268.74, 919.46, 449.02). The cluster is positioned directly underneath the tunnel and 43 cm from the south west edge of the deposition hole (to the centre of the cluster). Events in cluster E and F occur in a region characterised by high compressive stress in a volume associated with the S1 ray-path category on 8th June 2009 between 10:43 and 11:00 am.

Table 3-2. Spatial distribution of the 2 events located in Cluster C.

Event Date (D/M/Y)	Northing (m)	Easting (m)	Depth (m)
18/05/2009	269.45	919.57	455.04
29/09/2009	269.43	919.58	455.08
Mean	269.44	919.58	455.06

Table 3-3. Spatial distribution of the 7 events located in Cluster E.

Event Date (D/M/Y)	Northing (m)	Easting (m)	Depth (m)
08/06/2009	268.79	919.56	456.98
08/06/2009	268.86	919.58	457.04
08/06/2009	268.94	919.72	456.79
08/06/2009	268.91	919.51	457.34
08/06/2009	268.87	919.52	457.32
08/06/2009	268.82	919.60	456.88
08/06/2009	268.87	919.63	456.90
Mean	268.87	919.59	457.03

Table 3-4. Spatial distribution of the 13 events located in Cluster F.

Event Date (D/M/Y)	Northing (m)	Easting (m)	Depth (m)
08/06/2009	268.75	919.43	448.89
08/06/2009	268.72	919.41	449.01
08/06/2009	268.72	919.51	449.09
08/06/2009	268.81	919.44	449.10
08/06/2009	268.66	919.44	449.06
08/06/2009	268.75	919.49	448.98
08/06/2009	268.73	919.54	448.99
08/06/2009	268.77	919.47	449.07
08/06/2009	268.73	919.36	449.08
08/06/2009	268.70	919.48	449.01
08/06/2009	268.72	919.48	448.99
08/06/2009	268.79	919.42	448.92
Mean	268.74	919.46	449.02

Figure 3-16 shows plan views of events recorded during excavation, the initial phase of heating, the previous 2 years of monitoring and this monitoring period. The majority of the events are located in the NE and SW quadrants, i.e. position of clusters B, D, E and F. These regions are subject to increased compressive stresses, as identified from the in situ stress field by Pettitt et al. (1999). One event during this period is observed in the orthogonal regions of low-compressive or tensile stress. This pattern is consistent throughout the excavation and heating phases.

The events in Clusters B, C and D are located in the same volumes as clusters observed in previous monitoring periods and are thus interpreted as occurring along the same structures. The events could be a continuation of activity in the damaged zone, created either by movement on pre-existing micro-cracks or as a result of extension or formation of new microcracks in the existing damaged region. Similarly, Cluster E observed in this monitoring period occurs in a region where events have located previously during excavation.

Cluster F, defined in this monitoring period, is positioned in a region where events have not been previously located by the AE system but are close (30 cm) to event clusters recorded during excavation as shown in Figure 3-17. The events are close to the tunnel and so are expected to be in a region which was damaged when the tunnel was excavated. The region also coincides with high compressive stresses found to the south west of the deposition hole. The events occur on one day within the space of 20 minutes. No significant changes are observed in the temperature or pressure measurements during this time, but it is recommended that further instruments measuring environmental variables in the tunnel and deposition holes are studied to see if concurrent changes are observed.

Relative AE magnitudes for the five response periods discussed in Table 4-1 are displayed in Figure 3-18. Two events located during this monitoring period are greater than M=–1.10. The event with the greatest magnitude, –0.30, locates on the north west side of the deposition hole in an orthogonal region of low-compressive or tensile stress. The other large magnitude event, M=–1.02 occurs at cluster F. The peak magnitudes of the other 23 AE events are comparable to the previous report period and remain below the highest magnitudes observed in the initial phases of heating and pressurisation (response periods 1 and 2).

Although two new clusters of events are located during this period, their positions are consistent with pre-existing damaged zones, in which the continuation of activity in the damaged zone regions is thought to occur, and are small in number. Therefore we can assume that the rock mass around the deposition holes has remained relatively stable throughout this six-month period.

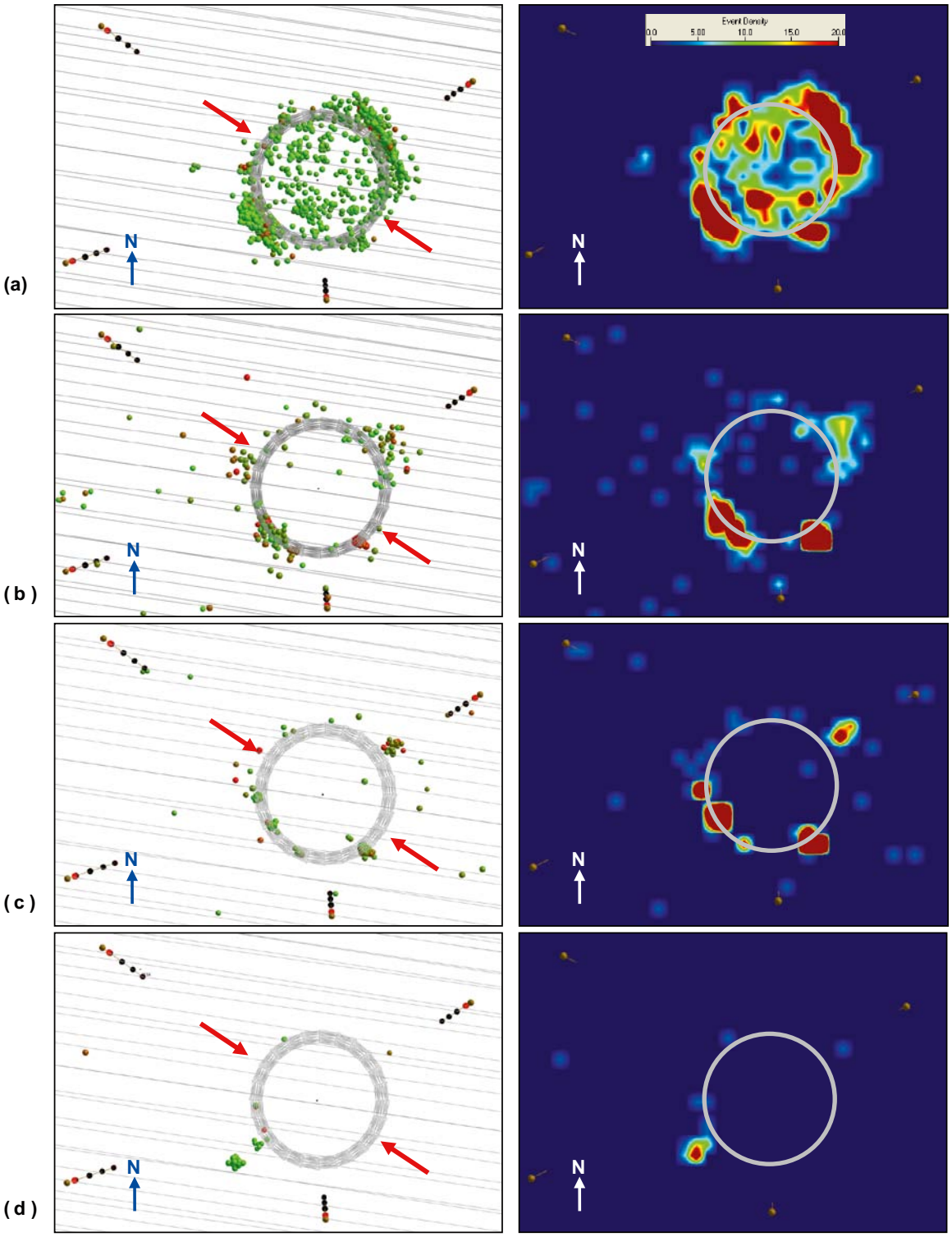

Figure 3-16. *Plan view of total AEs located around deposition hole DA3545G01 (right) and density plane plan view (left) during (a) the excavation phase (Pettitt et al. 1999), (b) monitoring during heating through to 01/04/2007, (c) previous monitoring from 01/04/2007 until 31/03/2009, and (d) this monitoring period from 01/04/2009 until 30/09/2009. The red arrows mark the orientation of principle stresses.*

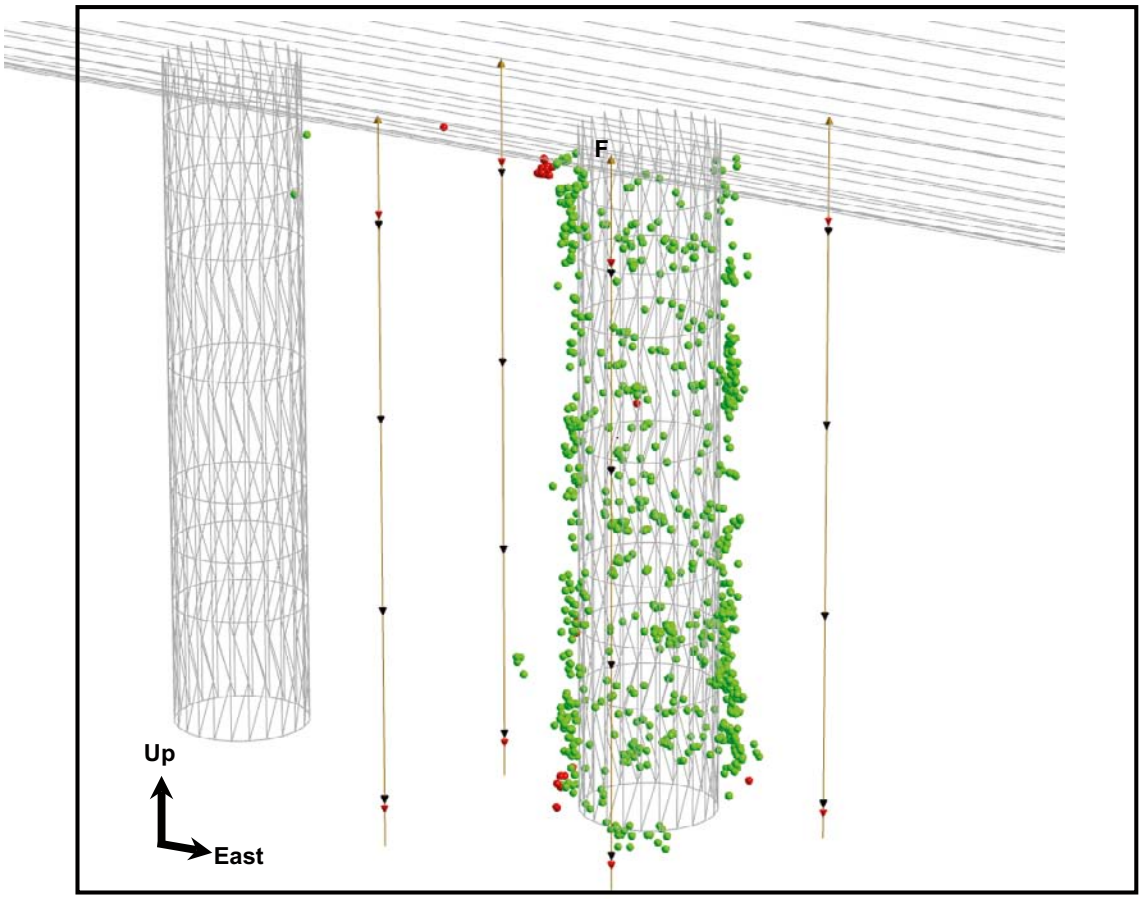

Figure 3-17. *Oblique view showing the clustered AE activity located around deposition hole DA3545G01. Green events are those located during excavation and red events are those located during this monitoring period. Cluster F, identified during this monitoring period, is labelled.*

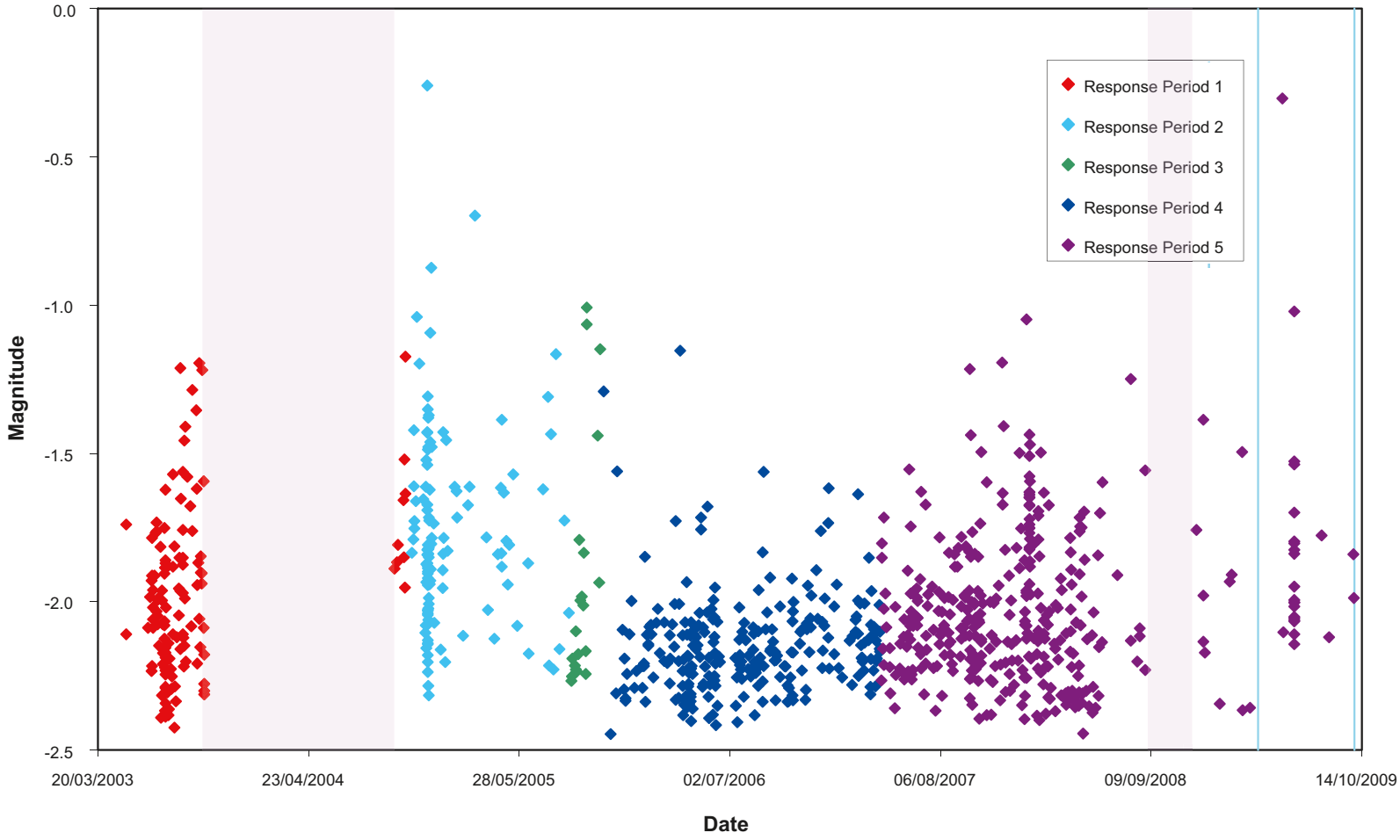

Figure 3-18. *Chart displaying AE magnitudes recorded from the beginning of heating and pressurisation. Events are coloured by response period as defined in Table 4-1. Periods when the AE system was not located on the Prototype experiment or not operational are designated by purple shading. The latest period is indicated by blue vertical lines.*

4 Conclusions

4.1 Monitoring between April 2009 and September 2009

- This report describes the results from acoustic emission (AE) and ultrasonic monitoring around a canister deposition hole (DA3545G01) in the Prototype Repository Experiment at SKB's Hard Rock Laboratory (HRL), Sweden. The monitoring aims to examine changes in the rock mass caused by an experimental repository environment, in particular due to thermal stresses induced from canister heating and pore pressure variation induced from tunnel sealing. Monitoring of this volume has been performed during excavation (Pettitt et al. 1999) and during stages of canister heating and tunnel pressurisation (Haycox and Pettitt 2005a, b, 2006a, b, Zolezzi et al. 2007, 2008, Duckworth et al. 2008, 2009, Haycox and Duckworth 2009). This report covers the period between 1st April 2009 and 30th September 2009 during which time the temperature of the rock surrounding deposition hole DA3545G01 has been very stable, and pressure around the deposition hole and in the backfill above the deposition hole has observed a steady increase.
- During this monitoring period there were a total of 25 AE events located with high confidence. A peak in activity occurs on 8th June 2009, when 19 events are located between 10:43 and 11:00 am. These events position in two clusters where significant activity has not been observed since deposition hole excavation. A cluster of seven events, defined as position E, is located towards the bottom, and on the south west side of the deposition hole. The events have average location N, E, D = (268.87, 919.59, 457.03), although they are not as tightly clustered, particular in depth. The second set of events, defined Cluster F, consists of 13 locations with average N, E, D = (268.74, 919.46, 449.02). The cluster is positioned directly underneath the tunnel and 43 cm from the south west edge of the deposition hole (to the centre of the cluster). Events in cluster E and F occur in a region characterised by high compressive stress in a volume associated with the S1 ray-path category.
- Cluster B consists of a single AE event in this period at N, E, D = (269.09, 919.70, 455.07). The event is located on the south west side of deposition hole DA3545G01 and has been observed in previous monitoring periods (Duckworth et al. 2008, 2009, Haycox and Duckworth 2009). The cluster occurs in a volume associated with the S1 ray-path category which passes through a region characterised by high compressive stress. Two events locate at Cluster C with a centre located at approximately N, E, D = (269.44, 919.58, 455.06) (Table 3-2). This cluster is at a similar depth to Cluster B but at the west side of the deposition hole, first classified by Duckworth et al. (2008). One event locates at the position of Cluster D during this period at N, E, D = (270.25, 921.58, 457.17). Cluster D occurs in the high compressive stress region diametrically opposite to clusters B and C during excavation (Figure 3-14). No events are observed to locate in Clusters A or T observed previously.
- The events in Clusters B, C and D are located in the same volumes as clusters observed in previous monitoring periods and are thus interpreted as occurring along the same structures. The events could be a continuation of activity in the damaged zone, created either by movement on pre-existing microcracks or as a result of extension or formation of new microcracks in the existing damaged region. Similarly, Cluster E observed in this monitoring period occurs in a region where events have located previously. Cluster F is positioned in a region where events have not been previously located by the AE system but are close (30 cm) to event clusters recorded during excavation. The events are close to the tunnel and so are expected to be in a region which was damaged when the tunnel was excavated. The region also coincides with high compressive stresses found to the south west of the deposition hole. From the relative lack of activity (e.g. compared to the excavation period) we conclude that the rock mass around the deposition holes has remained relatively stable throughout this six-month period.
- Ultrasonic surveying was not possible for transmitters 2 to 8 (inclusive) between 28th August 2009 and the end of the reporting period due to equipment malfunction. The malfunction was fixed on 4th November 2009. Consequently, measurements in the change of amplitude, velocity and rock properties are affected after 29th August 2009 as smaller numbers of ray-paths are used in the calculations, and certain ray-path categories, defined by Pettitt et al. (1999), no longer have data.

- The maximum change in average velocity is approximately +1.1 ms^{-1} for P-waves and approximately +0.3 ms^{-1} for S-waves, with average changes in the region of 0.5 ms^{-1} for P-waves and 0.1 ms^{-1} for S-waves. The changes in average velocity experienced in this period are therefore smaller than the estimated uncertainties (2 ms^{-1}) and not significant. P- and S-wave amplitudes remain relatively stable, within 0.07 dB of the amplitude at the start of the reporting period, until 21st June 2009 when P- and S-wave amplitude drops by 0.11 db and 0.10 db respectively over 8 days (a relatively large change for the period). The amplitudes generally remain lower than at the start of the monitoring period until 29th August 2009.
- The average velocity changes across each of the five ray-path categories are small and similar for P- and S-waves. Consequently, rock parameters show little variation for the same period. P- and S-wave amplitudes remain stable in April, May and June, but a decrease in amplitude occurs for all ray-path categories between 21st June and 29th June. The trend for the rest of the monitoring period is for little change in amplitudes. Category S1 ray-paths, passing through a volume of high compressive stresses, exhibit the greatest variation.
- There are little changes in the environmental conditions in the tunnel and around the deposition hole, so the AE rates and small variations in velocity and amplitude observed are a reflection of these static conditions. With no short-term changes in temperature and pressure this report period is comparably stable.

4.2 Summary of monitoring from the heating and pressurisation phase

- Monitoring of the heating and pressurisation phase at the Prototype Repository Experiment has been conducted since March 2003. Analysis of the AEs and ultrasonic measurements is split into five response periods (following previous reports). Table 4-1 presents a summary of the observations from ultrasonic monitoring thus far and Table 4-2 provides interpretations of the rock response.
- Figure 4-1 shows average P- and S-wave velocity and amplitude measurements recorded since the start of monitoring for the heating and pressurisation phase.
- Figure 4-2 to Figure 4-6 provide average velocity and modulus changes for the six ray-path categories selected in terms of disturbed and damaged regions. Figure 4-7 and Figure 4-8 show all locations and the temporal distributions of located AEs recorded since March 2003. Figure 4-9. The rate of AE activity around the deposition hole has been observed to significantly decrease from June 2008. This coincides with a decrease in temperature from approximately 53ºC to 44ºC.
- Figure 4-13 summarise changes that take place at different regions around the deposition hole in schematic diagrams for each period, identifying the primary changes in the properties of the rock as described in Table 4-2. The relatively low number of AEs and continuing trend of decreasing AE activity throughout response period 5 suggests the rock mass is becoming increasingly more stable as the experiment continues. The cumulative located events rate Figure 4-8 shows a marked change after 9th April 2008. The reduction in gradient of the line, ignoring the period when the system was offline for refurbishment and the spike on 8th June 2008, indicates a reduction in the number of AEs occurring. This reduction in average number of events per day recorded during the past eighteen months (Table 3-1) further supports the stabilisation of the rock mass. This reduction in activity must be related to stress and/or environmental conditions in the repository, which should be further investigated as it could lead to important geomechanical observations that could be fed back into future repository designs.

4.3 Recommendations

The rock mass around the deposition holes has remained relatively stable during this monitoring period.

- Two clusters, where significant activity has not been observed since deposition hole excavation, exhibit activity during this reporting period (defined as E and F in Figure 3-13). The cluster of seven events at position E is located towards the bottom, and the south west side, of the deposition hole. Cluster F consists of 13 events positioned directly underneath the tunnel and 43 cm from the south west edge of the deposition hole (to the centre of the cluster). Events in cluster E and F occur in a region characterised by high compressive stress in a volume associated with the S1 ray-path category on 8th June 2009 between 10:43 and 11:00 am. Temperature and pressure measurements used in this report do not show significant changes between the 8th and 9th June. Data from the full range of instruments available at the Prototype Repository could be investigated to determine whether anomalies occur at this time that may explain the initiation of activity.

Table 4-1. Summary of velocity, amplitude and AE variation measured during five response periods of temperature and/or pressure change.

Name/Date	Temperature/Pressure	Velocity	Amplitude	AE
PERIOD 1 25th May 2003 to 31st October 2004	Heaters in canister switched on causing an initially rapid change in temperature which gradually levels out to a constant increase. An increase of 35ºC is measured for an instrument in rock adjacent to the deposition hole. Pressure constant.	Rapid increase in P- and S-wave velocity on S3 category. Other categories show increases but to a lesser extent. Initial decrease in P-wave velocity in comparison to S-wave velocity for all ray-paths except for S3.	Amplitudes increase over this period by between 3 dB and 9 dB for P-wave amplitude, and 7 dB and 12 dB for S-wave amplitude.	AEs do not start immediately after heating. This could be a Kaiser-type effect in which AE rate remains close to background level until stress increases above the largest previous value. Peak of 13 events located on 26th June 2003. Average Event Rate = 0.5/day.
PERIOD 2 1st November 2004 to 4th September 2005	Drainage to tunnel closed on 1st November. Pressure in tunnel increases. Pressure increases measured in the deposition-hole buffer between 3rd and 5th December. Damage observed on canister on 6th December so drainage reopened and heaters switched off. Power switched on 15th December.	Velocity increases measured close to the tunnel from 26th November. Larger increases measured on categories S1 and S3.	Amplitude increases measured close to the tunnel from 26th November.	Relatively large number of events recorded in this period. Peak rate of 32 AEs on 4th and 5th December. Events locate in clusters in previously observed damage zone. Average Event Rate = 0.4/day.
PERIOD 3 5th September 2005 to 2nd November 2005	Additional drainage is opened in August 2005 leading to a decrease in pressure and temperature. Heaters turned off on 5th September.	P- and S-wave velocities decrease on all ray-path categories except Far.	P-wave amplitude decrease on all category ray-paths.	Slight increase in event rate above background rate recorded in previous 5 months. Average Event Rate = 0.3/day.
PERIOD 4 3rd November 2005 to 13th April 2007	Pressure in tunnel increases. Constant increase in pressure in buffer above deposition hole. Heaters switched on again so temperature around the deposition hole increases.	P- and S-wave velocities increase on all category ray-paths. Larger increases measured on S3.	P- and S-wave amplitude increase on the majority of ray-paths.	Cluster of 202 events located on SE side of deposition hole. Similar rate of AE locations. Average Event Rate = 0.46/day.
PERIOD 5 14th April 2007 to 30th September 2009	Short-term variations of pressure and temperature in the tunnel and deposition hole. Missing pressure data period (24/06/2007–09/09/2007). Missing ultrasonic data periods (17/12/2007–27/07/2008 and 30/08/2009–30/09/2009) Missing acoustic emission and ultrasonic data period (01/09/2008–27/11/2008).	P- and S-wave velocities generally increase on all category ray-paths. Larger increases measured on all ray-paths related to instrument 6. Largest decrease in October 2007 is observed on category C2.	P- and S-wave amplitudes increase on all ray-paths. Deviation observed during short-term pressure and temperature excursions.	377 events predominantly located in 4 distinct clusters on SE, SW and NE sides of deposition hole. Peak of 21 events on 22nd January 2008 locate in an anomalous cluster some distance from the deposition hole. Peak of 19 events on 8th June 2009 in two clusters on SW side of deposition hole. Average Event Rate = 0.46/day.

Table 4-2. Summary of key interpretation of rock response from the ultrasonic measurements.

Period	Summary of Key Interpretations
1	The heaters are switched on. The S3 category ray-paths pass through a volume that is unloaded and hence experiences low compressive stresses. This volume responds more rapidly to thermal stresses because existing microfractures are initially unloaded and hence more open than microfractures in the compressive region. P- and S-wave velocities decrease a similar amount during excavation as they increase during heating. This suggests very strongly that the microfractures induced in the regions of tensile damage around the deposition hole close when thermal stresses are applied. The difference in the rate of response between ray-paths in the compressive categories was interpreted as a different magnitude of response of the microfractures in the rock mass to increasing thermal stresses. In the first few months of heating, another effect is superimposed onto the rock's response to thermal stresses. This is measured as a reduction in P-wave velocities compared to S-wave velocities in the first few months of heating. This is particularly noticeable on S1 category in Figure 4-2, in which P-wave velocity decreases by about 3.5 ms^{-1} while S-wave velocity remains constant. A desaturation occurs on all ray-path categories other than S3. This must be caused by a drying of the rock mass, in the zones experiencing high compressive stresses, as heat is applied to the rock (i.e. both temperature and pressure are acting to expel moisture). In the low-compressed, or tensile, region saturation increases during this period. This is probably caused by hot fluids expanding into the open microfracture fabric.
2	Pressure rose rapidly after drainage from the tunnel was closed. This resulted in damage to the canister and the heaters being temporarily switched off. Temperature around the deposition hole dropped rapidly, but started increasing again after 13 days. Significant changes to the character of many recorded ultrasonic waveforms were observed as significant increases in signal quality. This suggests that as pressure increased in the rock surrounding the deposition hole, attenuation of the ultrasonic waves is significantly reduced meaning that they can pass more efficiently through the rock medium. The pressure increase can be interpreted as increasing the stiffness of the rock with a corresponding decrease in crack density. The magnitude of increase is greater for S1 and S3 categories because the volumes through which they pass are close to the deposition holes and contain a higher proportion of microfractures in an excavation damage zone. The pressure increase acts as a confining pressure on the rock mass leading to a closure of the pre-existing microcrack fabric and therefore a reduction in crack density. We observe that only a relatively small pressure increase is sufficient to close this microcrack fabric in the volumes already under high compressive stresses, leading to an initially high rate of change in measured velocities followed by a constant level, even though pressures may keep increasing afterwards. From Figure 4-2 the required pressure increase is approximately 1.5 MPa. The rapid pressure increase led to 32 events locating in clusters over the course of two days. The events are interpreted as stress changes in the rock as it responds to the sudden pressure change. This induces small scale movement on pre-existing microcracks, or induces new microfractures in weaker volumes of the rock. Pore pressure increases may also have assisted in inducing slip on pre-existing microfractures, by reducing the normal stress on the fractures. Over the rest of this period, as pressure continued to increase, fewer events were located. Another effect at this time is a rapid cooling of the rock when the heater inside the canister is switched off (for 13 days between 2nd and 15th December 2004), followed by warming as the rock is reheated. The majority of categories do not show a significant change in P- or S-wave velocity during this period indicating they are relatively insensitive to temperature changes at this time (i.e. when pressures are high). The exception is category S3, which exhibits a decrease in P- and S-wave velocity followed by an increase that mirrors the rate at which temperature changes (Figure 4-3). This category was found to be the most sensitive to thermal stresses during the initial stages of heating. When the rock cools, thermal stresses acting in this volume of low compressive (or slightly tensile) stresses reduce causing unloading of the microcracks. Microcracks close again when the rock is reheated and thermal stresses increase.
3	In September 2005 additional drainage from a permeable mat placed on the inner surface of the outer plug was opened, and heaters were switched off. This resulted in a cooling and de-pressurisation of the deposition hole. Neither temperature nor pressure reduced to the background level. The decrease in velocity on most ray-paths is generally low compared to the increases observed previously. An exception to this is category S3. This category is observed as the most sensitive. As temperature and pressure decreases, stresses again reduce in this volume causing microcracks to reopen and resulting in an increase in crack density and reduced stiffness of the rock. At the start of the period a sudden (over a few days), but relatively small change in velocity is observed, superimposed on the longer-term trends. We believe these are related to rapid changes in fluid pressure; a corresponding increase is observed at the end of the period (start of Period 4). For Period 3, an increase in Young's Modulus occurs which indicates a stiffening of the rock. This short term change is therefore likely to be a sudden reaction of the rock mass to the decrease in fluid pressure, perhaps caused by a general closing of microcracks caused by decreased pore pressures. The reverse is true for Period 4, when a pressure increase leads to a general opening of microcracks caused by increased pore pressures. This is believed to be a different response to long term trends from thermal stresses and general confining of the rock mass.

4	During the fourth period, heaters were turned back on once more causing temperature around the deposition hole to increase. Pressure increased rapidly again, probably caused by changes in the buffer temperature (changes in water volume caused by the temperature in combination with low hydraulic conductivity) (Goudarzi and Johannesson 2006). Velocity increases rapidly at first, then at a constant rate, following a similar pattern to the temperature and pressure. Ray-path category S3 exhibits the greatest increase in P- and S-wave velocity. Similar patterns are observed on S1 and C1, and to a lesser extent on C2. Velocity on the Far ray-path category remains constant throughout the period. When temperature and pressure start to increase the stiffness of the rock increases, particularly on S3. This is accompanied by a reduction in crack density. The associated increase in stiffness and decrease in crack density can be interpreted as the closing of existing microfractures and pore spaces as observed previously. This effect has continued to the current day. Few events have been located during Periods 3 and 4. A rapid decrease, and then increase, in pressure and temperature appears to have no significant effect on the number, or distribution, of AEs around the deposition hole. The AE rate marginally increased since February 2006 (Figure 4-8). The vast majority of events locate on a single cluster in the south-east of the deposition hole and at 455.1 m depth. The low number of AEs suggests the rock mass has stabilised. The high pressures result in a confining pressure being placed on the rock around the deposition hole and inhibit the movement on microcracks or macrofractures.
5	During the fifth response period the excavation of a new tunnel near the prototype tunnel resulted in a gap in pressure data (from 24th June until 9th September 2007). Pressure in the tunnel backfill generally increased through the period (by ~1.7 MPa) while the temperature has remained extremely stable (maximum change of only 1–2°C). Conditions in the buffer surrounding the canister remain fairly stable with the exception of two sudden drops in both temperature and pressure. The first occurred on 21st October 2007, when temperature dropped by ~5°C and pressure by ~8 MPa, these changes coincide with decreases in P- and S-wave velocity and amplitude. The second occurred on 10th June 2008, at a time when no ultrasonic survey data was captured. A small increase in the pressure in the backfill occurs on 22nd October 2008 when no ultrasonic survey data were actively captured. As temperature and pressure decreases, stresses reduce in the volume causing microcracks to reopen, resulting in an increase in crack density and reduced stiffness of the rock. It is unclear whether the drop in pressure, temperature, or an optimal combination of the two is responsible for the observed changes in velocity and amplitude, but both are likely to affect the stress field in some manner. In the first six months of this period (April 2007–September 2007) the velocity and amplitude for both P- and S-waves increase between 20th and 24th April 2007. P-waves show higher variation than S-waves. The most sensitive ray-paths to the changes are those related with sensor 6. Analysis of the different ray-paths reveal that category Far shows the maximum velocity changes for both P- and S- waves while category C1 shows minor changes. The minimum variation in signal amplitudes is observed for S3 category. In the following six months (October 2007–March 2008) velocity and amplitude for both P- and S-waves decrease for a period between 21st and 26th October 2007 then increase more gradually, with only minor variations observed, until the end of March 2008. P-wave velocity increases suddenly to a period high on 21st November 2007. The most sensitive ray-path categories (with most observable variation) are C2, S3 and to a lesser extent C1. Data for velocity and amplitude are not obtainable from ultrasonic surveys after 17th December 2007 due to a power malfunction. Between April 2008 and September 2008 we observe small changes in P-and S-wave amplitude and velocity, and changes in rock properties that are similar to the previous six months, although category C1 displays the most variation. In the following six months (October 2008–March 2009) we observe comparably smaller changes in P-and S-wave amplitude and velocity, and similarly smaller changes in rock properties to the previous six months. This trend of little change in velocity an amplitude continues through the next six months (April 2009–September 2009). When velocity and amplitude variations are compared from before and after the system refurbishment (that occurred between September and November 2008) there are signal amplitude changes that occur. This prompted the need for a new reference survey for cross-correlation purposes. The selected survey was taken on 28th November 2008. The AE rate for the whole of this response period is the same as for response period 4. However, there has been a decrease in activity over the two and a half years, with a rate of 0.70 / day in the first six months reducing to 0.14 / day in the most recent six months. Events generally locate in clusters around the deposition hole: three of these clusters are recurring in active volumes, one occurring in a volume around the canister deposition hole not previously seen, and two clusters representing a newly activated volume in the tunnel floor. The AE activity would suggest that new fracturing or movement on existing fractures is reducing with time. Blasting records for 2007–2008 gave no indication that nearby tunnel excavation is directly responsible for increases in activity; although a time dependent stress effect could play a role. The relatively low number of AEs and continuing trend of decreasing AE activity throughout response period 5 suggests the rock mass is becoming increasingly more stable during the relatively static environmental conditions.

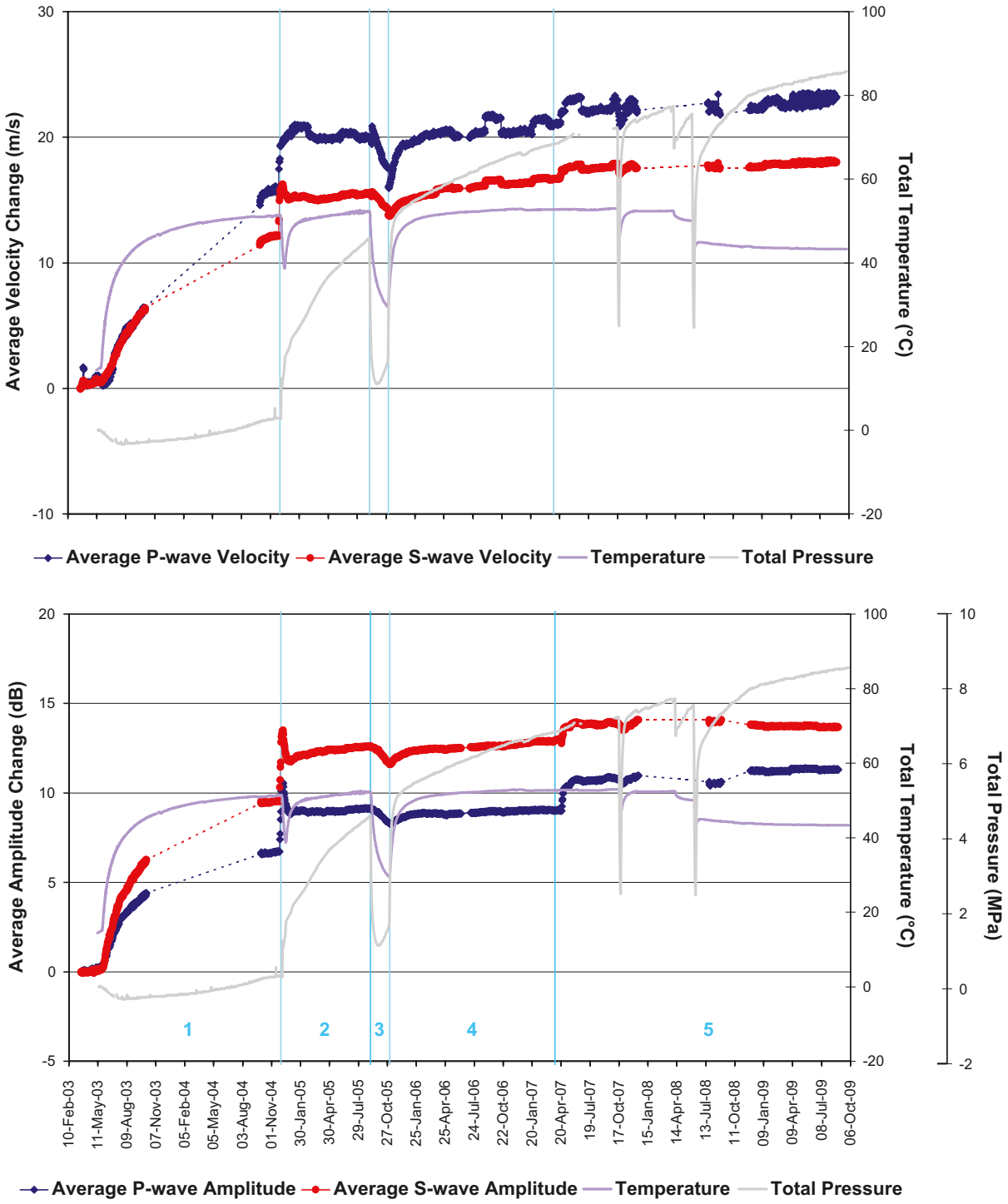

Figure 4-1. *P- and S-wave (a) velocity change and (b) amplitude change from the start of monitoring (20th March 2003), plotted alongside temperature (TR6045) and pressure (PB616) measurements in deposition hole DA3545G01. The vertical blue lines separate periods of similar environmental conditions as defined in Table 4-1.*

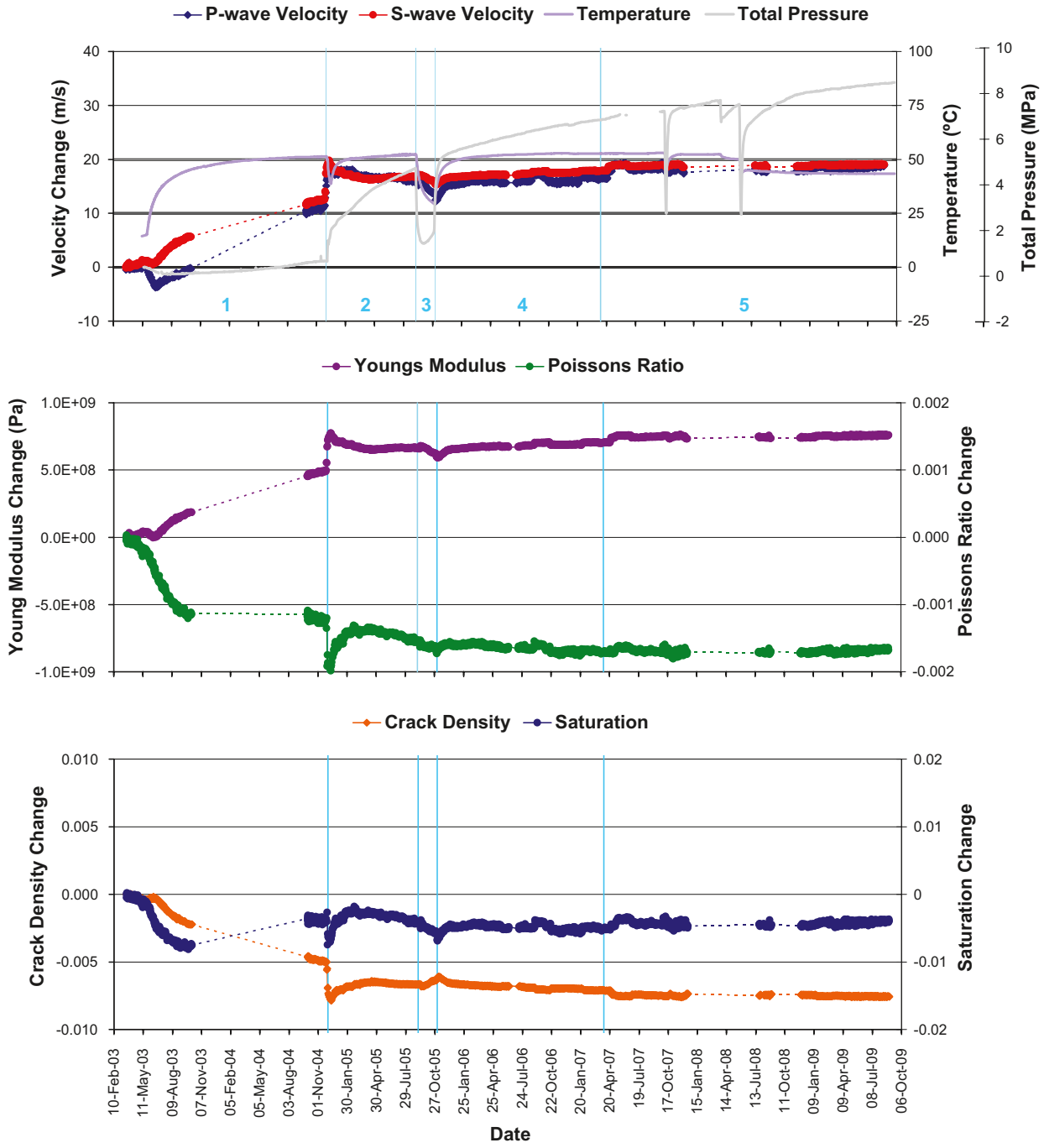

Figure 4-2. *Changes in rock properties and velocity along the S1 category of ray-paths. Average P- and S-wave velocity change shown with temperature (instrument TR6045) and total pressure (instrument PB616) (top), Young's Modulus and Poison's Ratio change (middle), and Crack Density and Saturation change (bottom). Periods representing similar environmental conditions, as defined in Table 4-1, are separated by the vertical blue lines.*

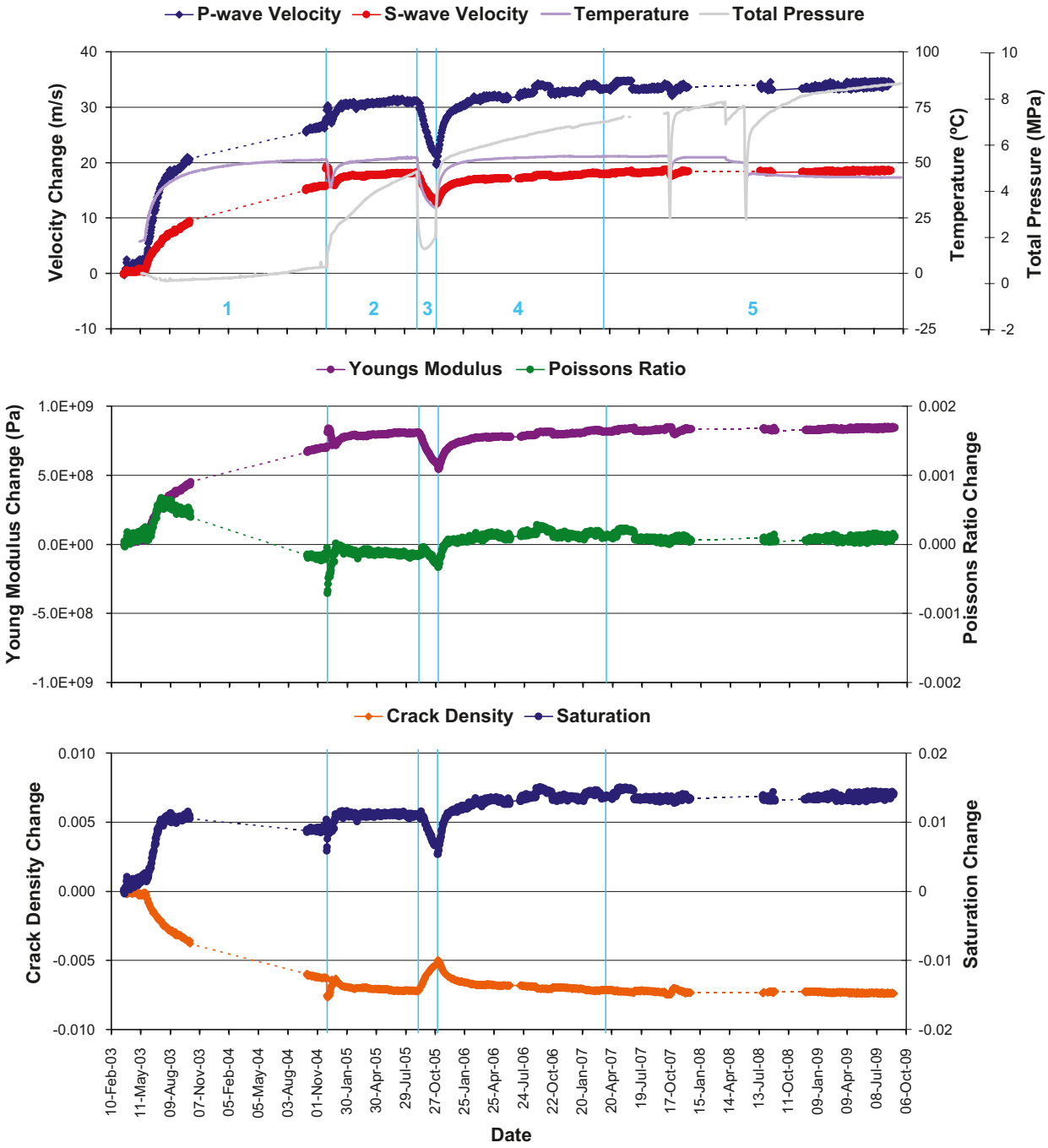

Figure 4-3. *Changes in rock properties and velocity along the S3 category of ray-paths. Average P- and S-wave velocity change shown with temperature (instrument TR6045) and total pressure (instrument PB616) (top), Young's Modulus and Poison's Ratio change (middle), and Crack Density and Saturation change (bottom). Periods representing similar environmental conditions, as defined in Table 4-1, are separated by the vertical blue lines.*

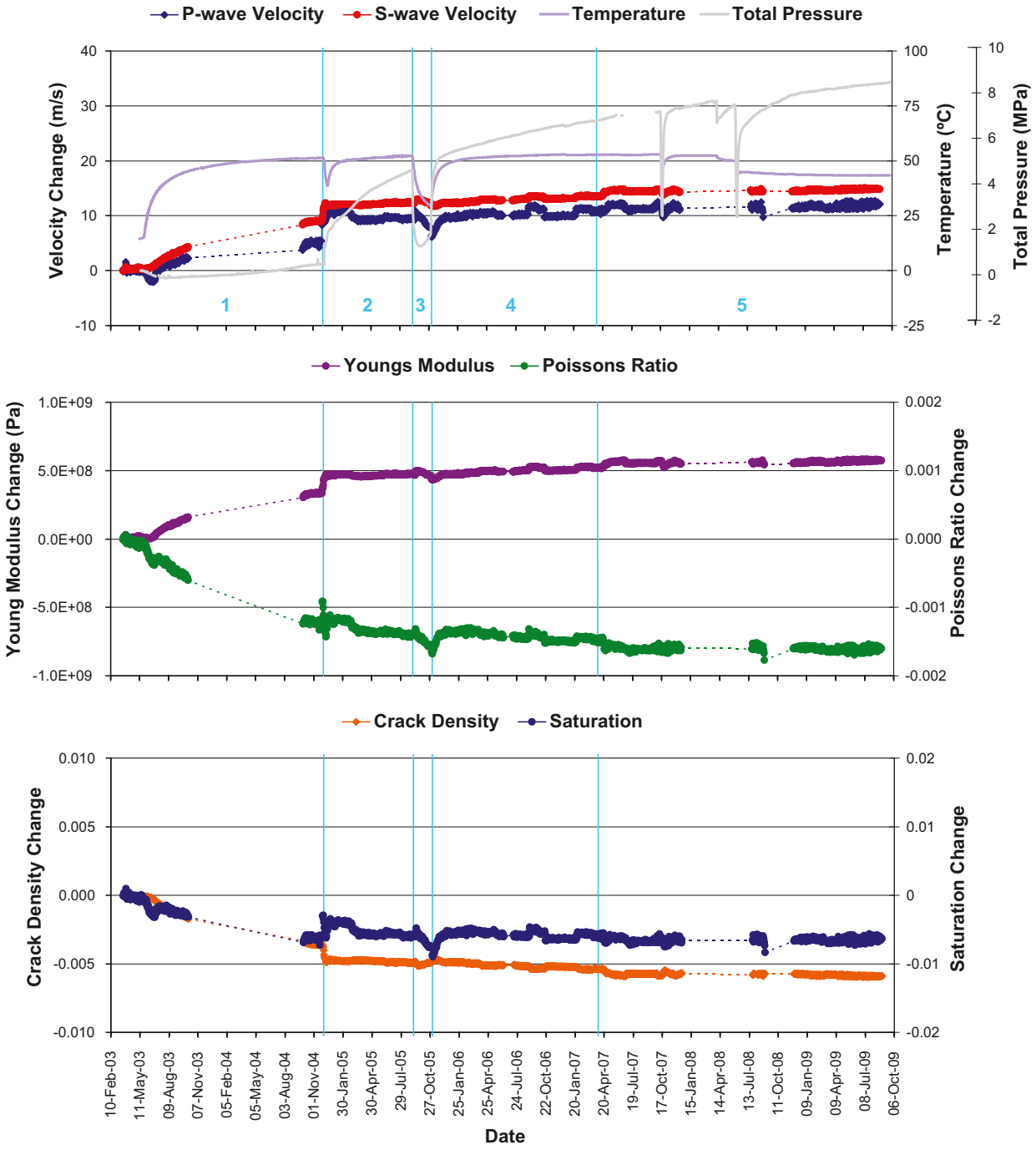

Figure 4-4. *Changes in rock properties and velocity along the C1 category of ray-paths. Average P- and S-wave velocity change shown with temperature (instrument TR6045) and total pressure (instrument PB616) (top), Young's Modulus and Poison's Ratio change (middle), and Crack Density and Saturation change (bottom). Periods representing similar environmental conditions, as defined in Table 4-1, are separated by the vertical blue lines.*

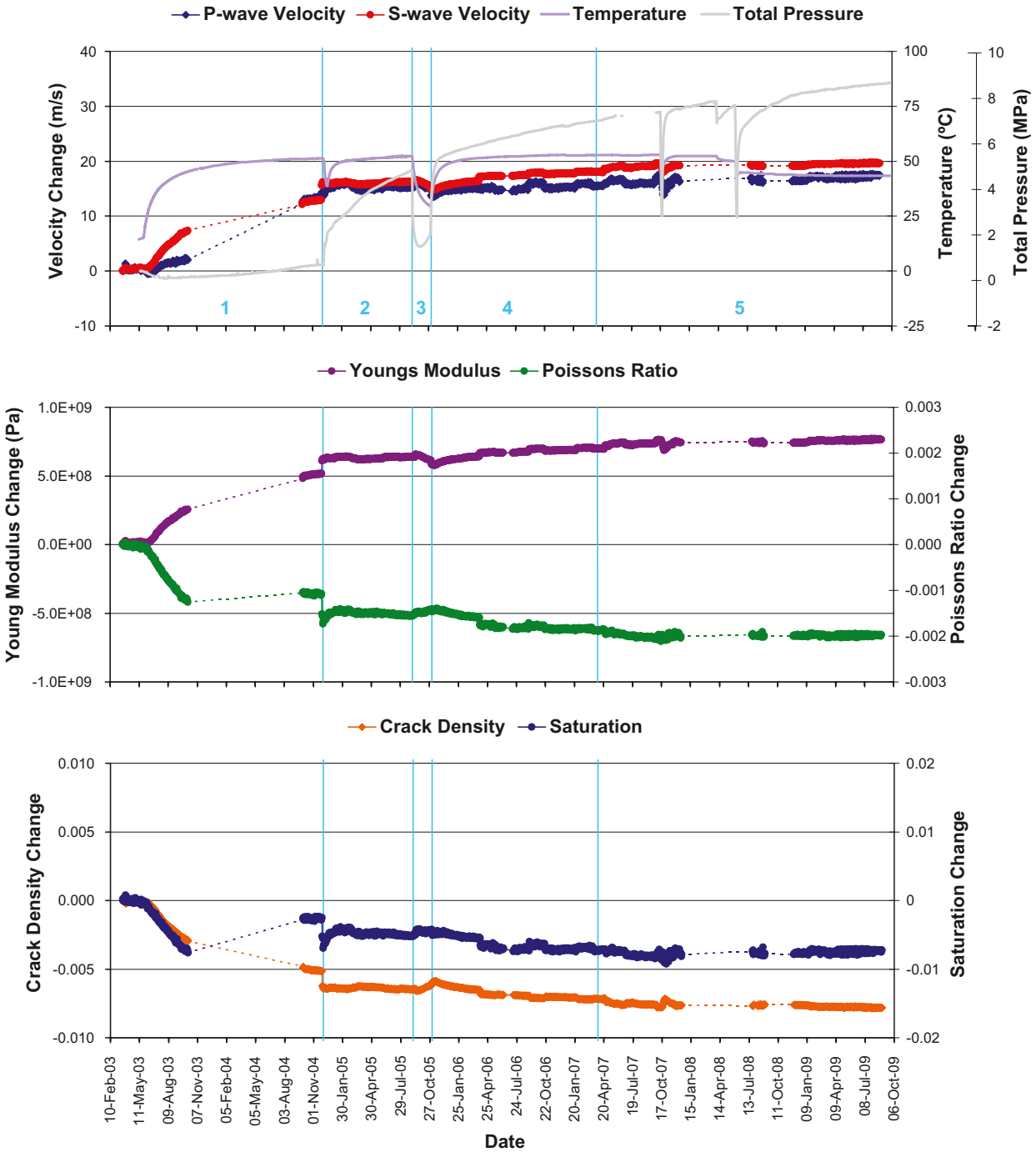

Figure 4-5. *Changes in rock properties and velocity along the C2 category of ray-paths. Average P- and S-wave velocity change shown with temperature (instrument TR6045) and total pressure (instrument PB616) (top), Young's Modulus and Poison's Ratio change (middle), and Crack Density and Saturation change (bottom). Periods representing similar environmental conditions, as defined in Table 4-1, are separated by the vertical blue lines.*

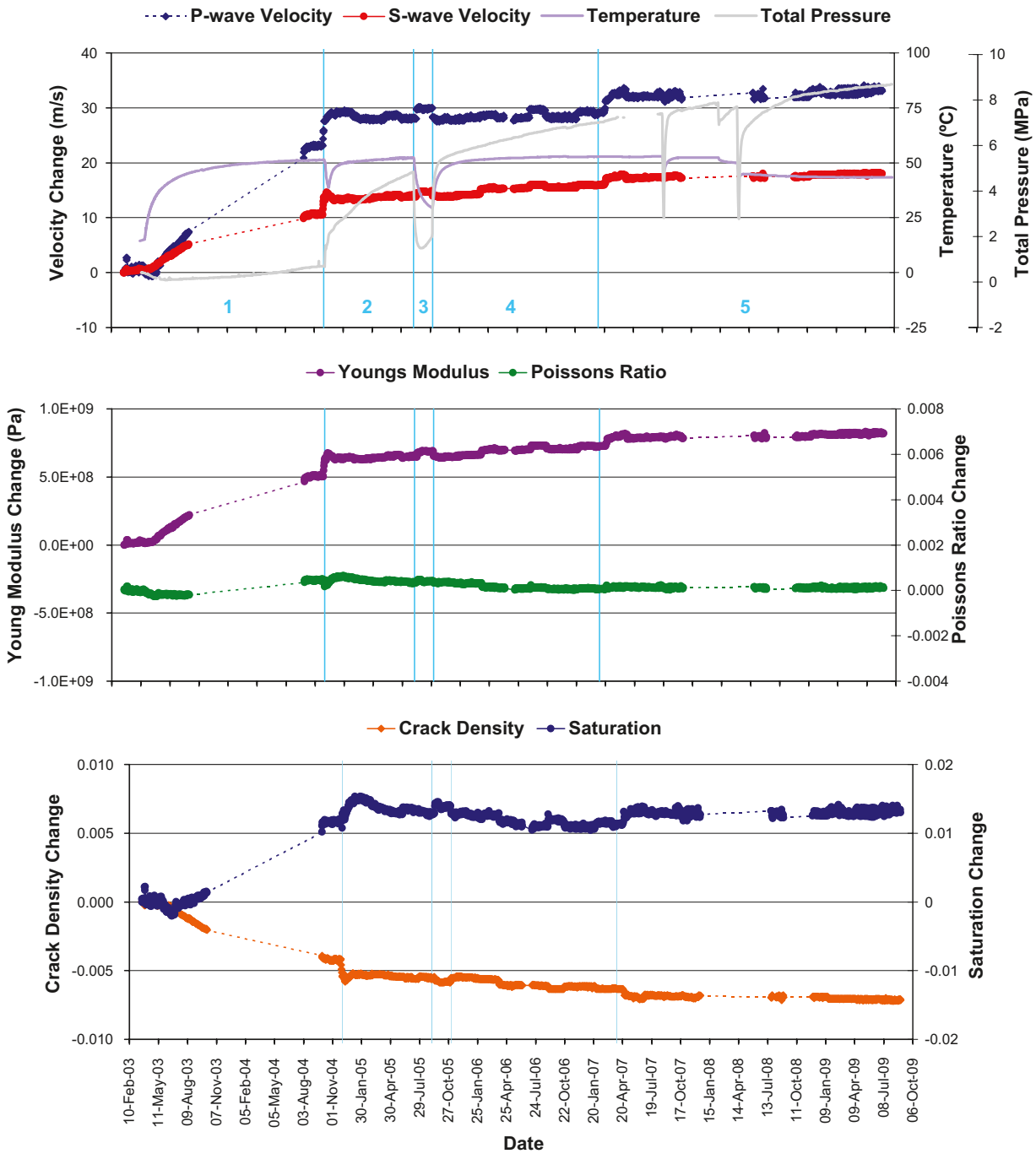

Figure 4-6. *Changes in rock properties and velocity along the Far category of ray-paths. Average P- and S-wave velocity change shown with temperature (instrument TR6045) and total pressure (instrument PB616) (top), Young's Modulus and Poison's Ratio change (middle), and Crack Density and Saturation change (bottom). Periods representing similar environmental conditions, as defined in Table 4-1, are separated by the vertical blue lines.*

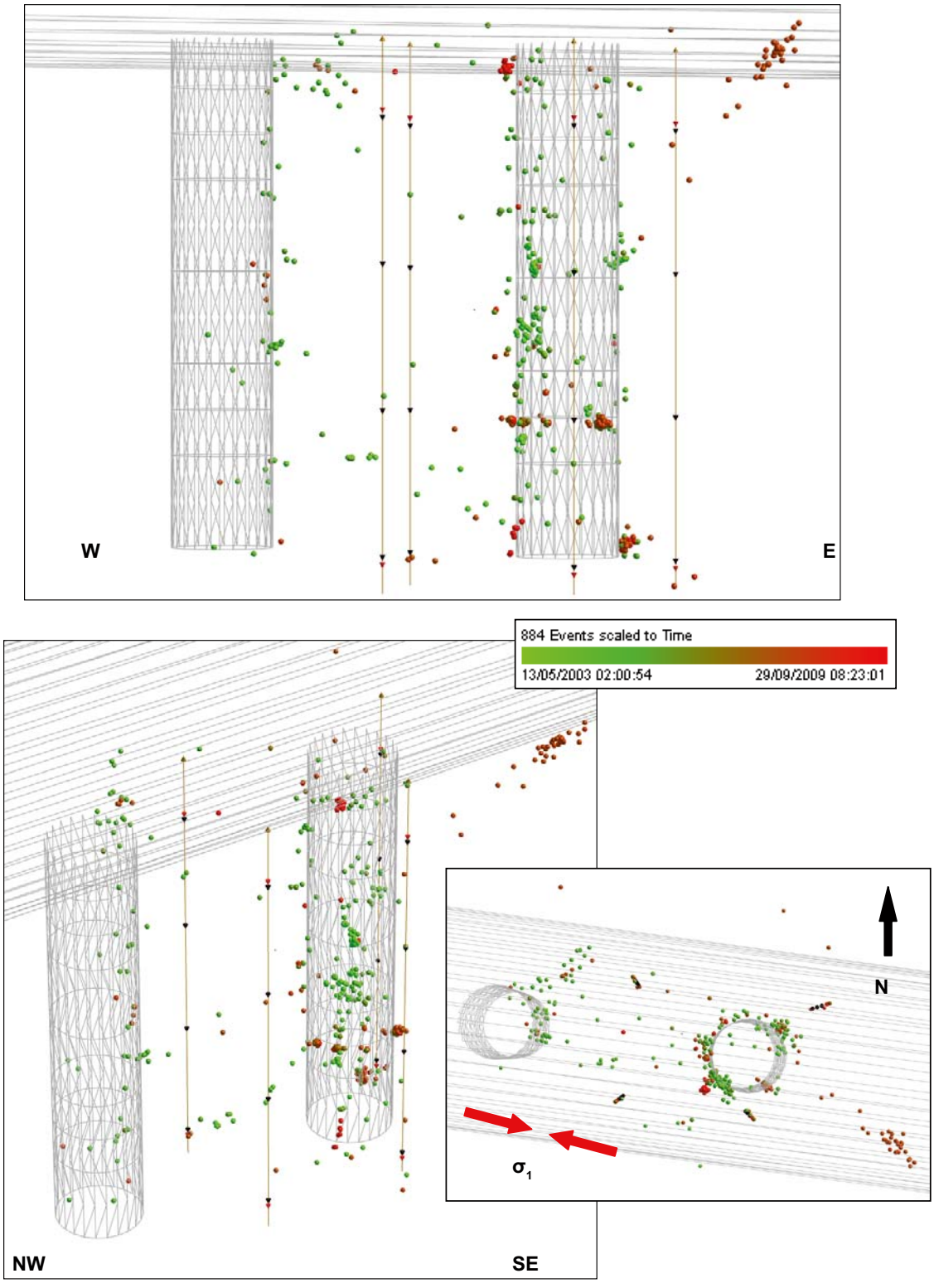

Figure 4-7. *Projections of all AEs located during the heating phase (20th March 2003 to 30th September 2009). In total there have been 884 events over the last six years of monitoring (events are scaled by time: green early and red late).*

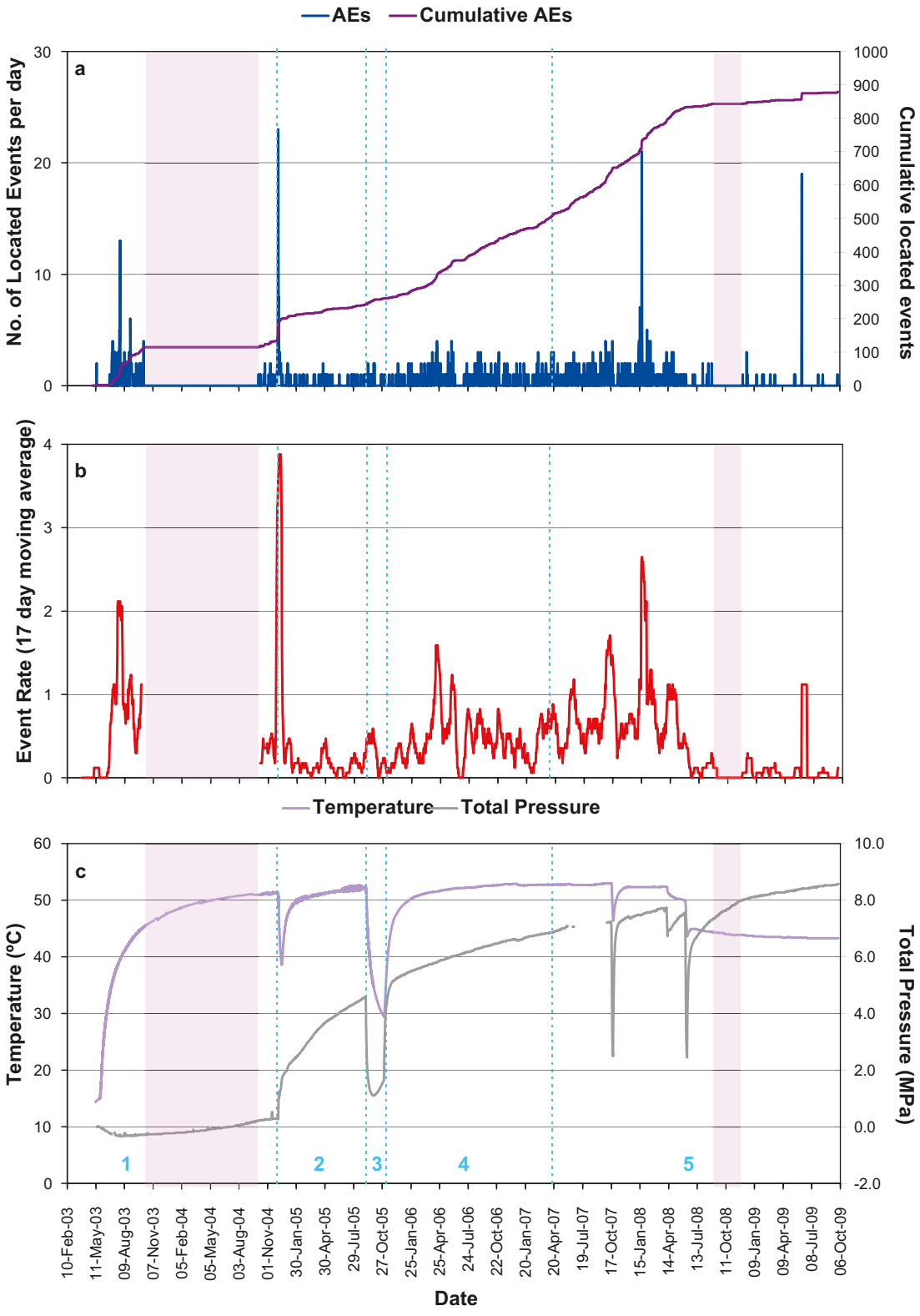

Figure 4-8. *(a) Number and cumulative number of located events from the start of monitoring in March 2003, (b) 17 day moving average of located AEs and (c) temperature (TR6045) and pressure (PB616) measurements in deposition hole DA3545G01. Periods representing similar environmental conditions, as defined in Table 4-1, are separated by the vertical blue lines. Times when the AE system was not located on the Prototype experiment or not operational are designated by purple shading.*

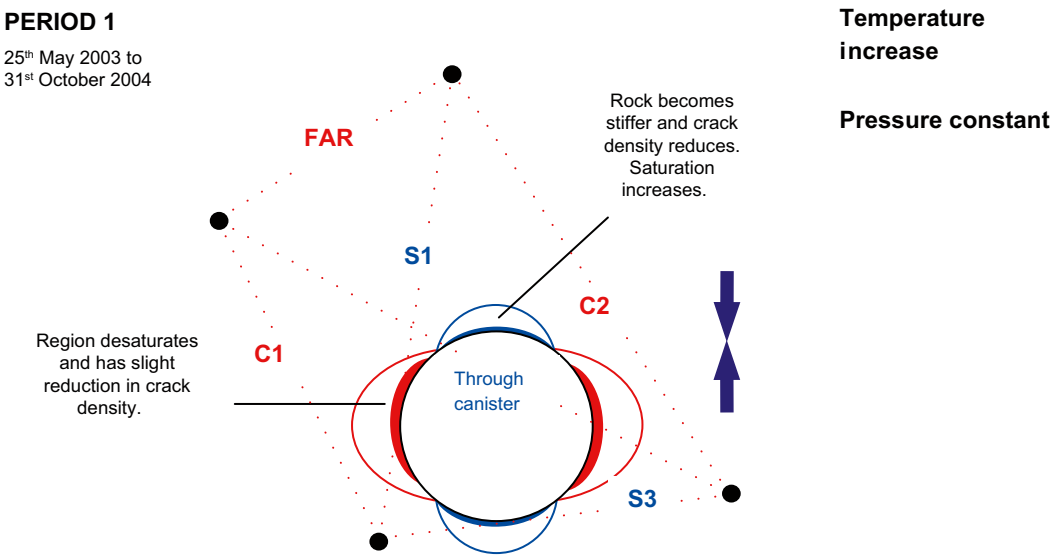

Figure 4-9. *Schematic diagram of the deposition hole and explanation of changes experienced during Period 1.*

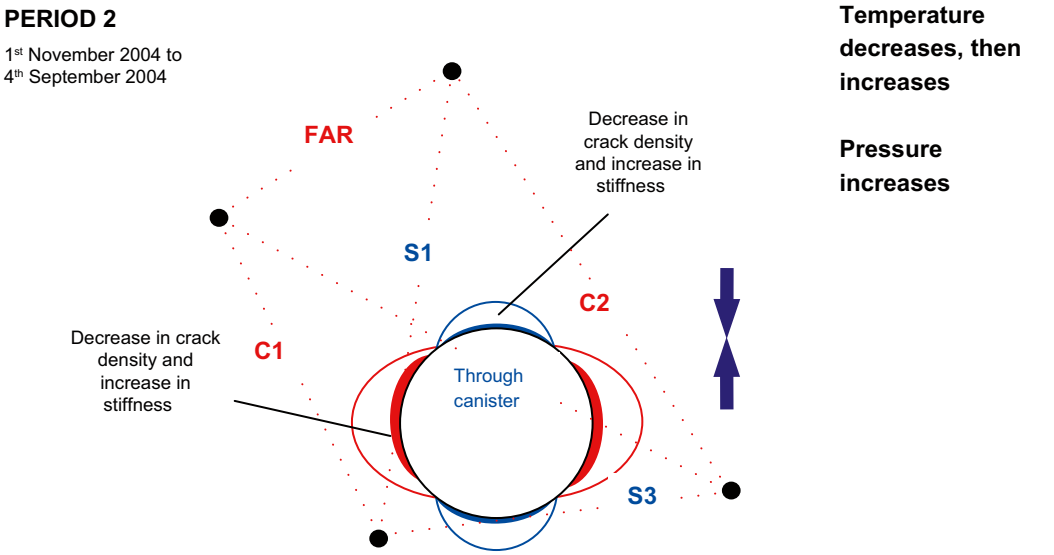

Figure 4-10. *Schematic diagram of the deposition hole and explanation of changes experienced during Period 2.*

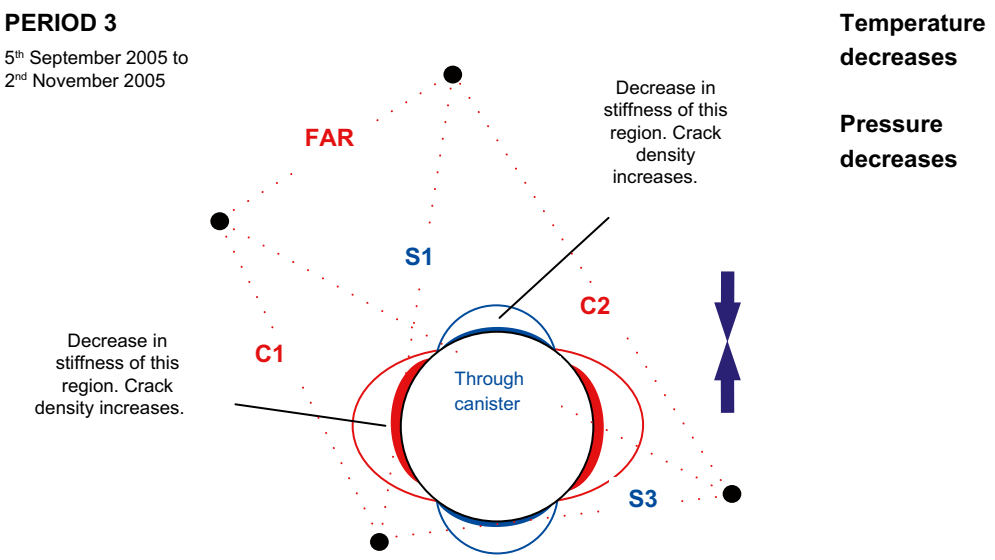

Figure 4-11. Schematic diagram of the deposition hole and explanation of changes experienced during Period 3.

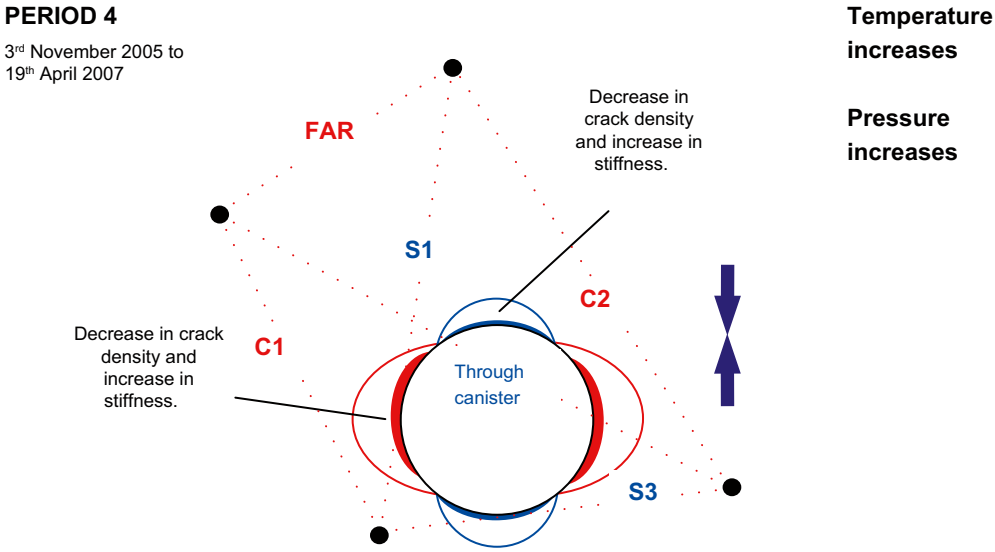

Figure 4-12. Schematic diagram of the deposition hole and explanation of changes experienced during Period 4.

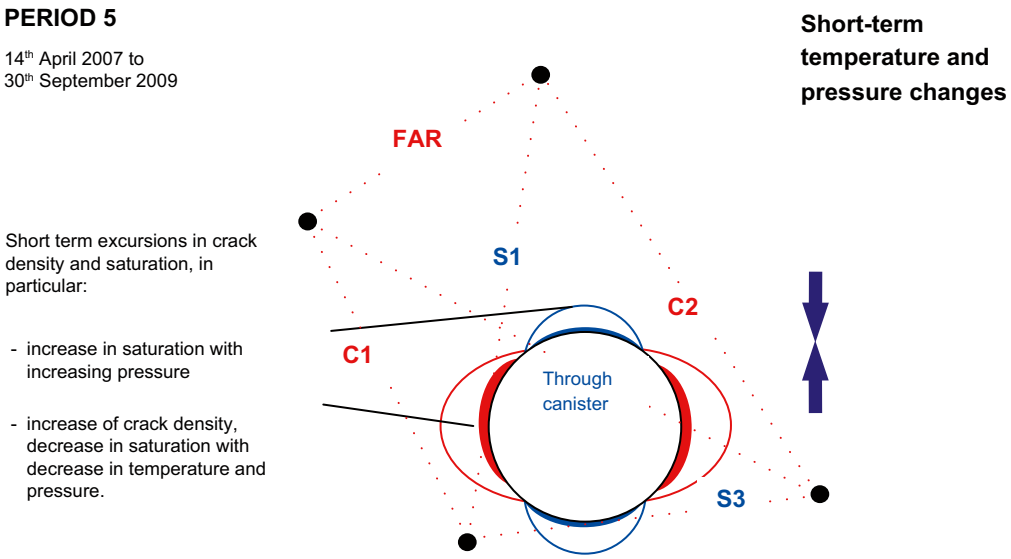

Figure 4-13. *Schematic diagram of the deposition hole and explanation of changes experienced during Period 5.*

References

SKB's (Svensk Kärnbränslehantering AB) publications can be found at www.skb.se/publications.

Duckworth D, Haycox J R, Pettitt W S, 2008. Äspö Hard Rock Laboratory. Prototype Repository. Acoustic emission and ultrasonic monitoring results from deposition hole DA3545G01 in the Prototype Repository between October 2007 and March 2008. SKB IPR-09-10, Svensk Kärnbränslehantering AB.

Duckworth D, Haycox J R, Pettitt W S, 2009. Äspö Hard Rock Laboratory. Prototype Repository. Acoustic emission and ultrasonic monitoring results from deposition hole DA3545G01 in the Prototype Repository between April 2008 and September 2008. SKB IPR-09-13, Svensk Kärnbränslehantering AB.

Goudarzi R, Johannesson L-E, 2006. Äspö Hard Rock Laboratory. Prototype Repository. Sensors data report (Period 010917–061201). Report No: 16. SKB IPR-07-05, Svensk Kärnbränslehantering AB.

Haycox J R, Duckworth D, 2009. Acoustic emission and ultrasonic monitoring results from deposition hole DA3545G01 in the Prototype Repository between October 2008 and March 2009. SKB P-11-29, Svensk Kärnbränslehantering AB.

Haycox J R, Pettitt W S, 2005a. Äspö Hard Rock Laboratory. Prototype Repository. Acoustic emission and ultrasonic monitoring during the heating of deposition hole DA3545G01 in the Prototype Repository to March 2005. SKB IPR-05-30, Svensk Kärnbränslehantering AB.

Haycox J R, Pettitt W S, 2005b. Äspö Hard Rock Laboratory. Prototype Repository. Acoustic emission and ultrasonic monitoring results from deposition hole DA3545G01 in the Prototype Repository between April 2005 and September 2005. SKB IPR-05-31, Svensk Kärnbränslehantering AB.

Haycox J R, Pettitt W S, 2006a. Äspö Hard Rock Laboratory. Prototype Repository. Acoustic emission and ultrasonic monitoring results from deposition hole DA3545G01 in the Prototype Repository between October 2005 and March 2006. SKB IPR-06-23, Svensk Kärnbränslehantering AB.

Haycox J R, Pettitt W S, 2006b. Äspö Hard Rock Laboratory. Prototype Repository. Acoustic emission and ultrasonic monitoring results from deposition hole DA3545G01 in the Prototype Repository between April 2006 and September 2006. SKB IPR-06-36, Svensk Kärnbränslehantering AB.

Maxwell S C, Young R P, 1995. A controlled in situ investigation of the relationship between stress, velocity and induced seismicity. Geophysical Research Letters 22, 1049–1052.

Patel S, Dahlström L-O, Stenberg L, 1997. Äspö Hard Rock Laboratory. Characterisation of the rock mass in the Prototype Repository at Äspö HRL. Stage 1. SKB Progress Report HRL-97-24, Svensk Kärnbränslehantering AB.

Pettitt W S, Young R P, 2007. InSite seismic processor – user operations manual version 2.14. Applied Seismology Consultants, Shrewsbury, UK.

Pettitt W S, Baker C, Young R P, 1999. Äspö Hard Rock Laboratory. Prototype Repository. Acoustic emission and ultrasonic monitoring during the excavation of deposition holes in the Prototype Repository. SKB IPR-01-01, Svensk Kärnbränslehantering AB.

Pettitt W S, Baker C, Young R P, 2000. Äspö Hard Rock Laboratory. Analysis of the in situ principal stress field at the HRL using acoustic emission data. SKB IPR-01-09, Svensk Kärnbränslehantering AB.

Pettitt W S, Baker C, Young R P, Dahlström L-O, Ramqvist G, 2002. The assessment of damage around critical engineering structures using induced seismicity and ultrasonic techniques. Pure and Applied Geophysics 159, 179–195.

SKB, 1999. Äspö Hard Rock Laboratory. Current research projects 1998. Svensk Kärnbränslehantering AB.

Telford W M, Geldart L P, Sheriff R E, 1990. Applied geophysics. 2nd ed. Cambridge: Cambridge University Press.

Young R P, Pettitt W S, 2000. Investigating the stability of engineered structures using acoustic validation of numerical models. In: Labuz J F, Glaser S D, Dawson E (eds). Trends in rock mechanics: proceedings of sessions of Geo-Denver 2000, Denver, Colorado, 5–8 August 2000. Reston, VA: American Society of Civil Engineers. (Geotechnical Special Publication 102), pp 1–15.

Zimmerman R W, King M S, 1985. Propagation of acoustic waves through cracked rock. In Ashworth E (ed). Research & engineering applications in rock masses: proceedings of the 26th U.S. Symposium on Rock Mechanics, South Dakota School of Mines & Technology, Rapid City, 26–28 June 1985. Boston: A.A. Balkema, 739–745.

Zolezzi F, Haycox J R, Pettitt W P, 2007. Äspö Hard Rock Laboratory. Prototype Repository. Acoustic emission and ultrasonic monitoring results from deposition hole DA3545G01 in the Prototype Repository between October 2006 and March 2007. SKB IPR-07-12, Svensk Kärnbränslehantering AB.

Zolezzi F, Haycox J R, Pettitt W P, 2008. Äspö Hard Rock Laboratory. Prototype Repository. Acoustic emission and ultrasonic monitoring results from deposition hole DA3545G01 in the Prototype Repository between April 2007 and September 2007. SKB IPR-09-03, Svensk Kärnbränslehantering AB.

Appendix 1

Previous monitoring at the prototype repository

Ultrasonic monitoring has been conducted at the Prototype Repository since September 1999. During excavation, monitoring of both deposition holes in Tunnel Section 2 (DA3551G01 and DA3545G01) was undertaken to delineate zones of stress related fracturing and quantitatively measure fracturing in the damaged zone (Pettitt et al. 1999). Monitoring has been undertaken on a single deposition hole (DA3545G01) since 2003, and the response of the surrounding rock to changes in temperature and pressure has been measured with reporting of results every six months (see Table A1-1). This report presents new results from the period 1st April 2009 to 30th September 2009.

A temporary ultrasonic array was installed around the rock volume when deposition hole DA3545G01 and its neighbour DA3551G01, were first excavated in September 1999 (Pettitt et al. 1999). A total of 2,467 AE triggers were obtained during monitoring of the two deposition holes. Of these 1,153 were located. There was significantly more AE activity around the second deposition hole (labelled DA3545G01) than the first (DA3551G01). This difference is likely to depend upon intersection of the excavation with a greater number of pre-existing fractures. These fractures may be preferentially located in the side wall of the deposition hole or preferentially orientated to the *in situ* stress field. Fracturing associated with excavation-induced stresses was observed with AEs distributed mainly in regions orthogonal to the maximum principal stress, σ_1. This was consistent with observations from the Canister Retrieval Tunnel and from dynamic numerical models. AEs, and hence microcrack damage, were shown to locate in clusters down the deposition hole and not as a continuous 'thin skin'. Pettitt et al. (2000) showed that these clusters were associated with weaknesses in the rock mass generated by excavation through pre-existing fractures. Damage in the side wall of the deposition holes depended significantly on these pre-existing features. The *in situ* stress field was a contributing factor in that induced stresses were sufficiently high to create damage in these weakened regions although not sufficiently high to create significant damage in the rock mass as a whole.

A permanent ultrasonic array, with transducers grouted into instrumentation boreholes, was installed in the rock mass in June 2002. In this arrangement, ultrasonic monitoring has been conducted between 20th March and 9th October 2003, and then from 29th September 2004 to the present. A gap in monitoring occurred when the ultrasonic acquisition system was used for another experiment in the HRL (Pillar Stability Experiment). Processing and reporting of results has been undertaken, as shown in Table A1-1, and is further discussed in Section 4.2. A description of instruments measuring other environmental factors (such as temperature and pressure) and their locations can be found in Goudarzi and Johannesson (2006).

Table A1-1. Summary of ultrasonic monitoring at the Prototype Repository to-date.

Report	Monitoring Period	Location	Response Period
Pettitt et al. 1999	25/08/1999 to 18/09/1999	DA3551G01 and DA3545G01	Excavation
Haycox and Pettitt 2005a	20/03/2003 to 09/10/2003	DA3545G01	1
	29/04/2004 to 31/03/2005	DA3545G01	1, 2
Haycox and Pettitt 2005b	01/04/2005 to 30/09/2005	DA3545G01	2, 3
Haycox and Pettitt 2006a	01/10/2005 to 31/03/2006	DA3545G01	3, 4
Haycox and Pettitt 2006b	01/04/2006 to 30/09/2006	DA3545G01	4
Zolezzi et al. 2007	01/10/2006 to 31/03/2007	DA3545G01	4
Zolezzi et al. 2008	01/04/2007 to 31/09/2007	DA3545G01	4,5
Duckworth et al. 2008	01/10/2007 to 31/03/2008	DA3545G01	5
Duckworth et al. 2009	01/04/2008 to 30/09/2008	DA3545G01	5
Haycox and Duckworth 2009a	01/10/2008 to 31/03/2009	DA3545G01	5
Haycox and Pettitt 2009 (this report)	01/04/2009 to 30/09/2009	DA3545G01	5

Appendix 2

Methodology

Data acquisition

The ultrasonic array consists of twenty-four ultrasonic transducers configured as eight transmitters and sixteen receivers installed into four instrumentation boreholes. The transducers are fixed into the boreholes using specially designed frames (Figure A2-1) – two transmitters and four receivers per frame. The boreholes are vertical, 76 mm in diameter and approximately 10 metres in length distributed around each deposition hole volume. The array has been designed to provide good coverage for AE locations and to provide 'skimming' ray-paths that pass within a few centimetres of the deposition-hole void so as to sample the rock immediately adjacent to the deposition-hole wall. The layout of the instrumentation boreholes is shown in Figure A2-2 and described further in Table A2-1. Each of the ultrasonic transducers has a hemispherical brass cap fixed over its active face and is then spring-loaded against the borehole surface so as to obtain good coupling to the rock mass. The boreholes have then been filled with a slightly expansive grout so as to permanently fix the transducers in place, reduce the likelihood of damage to the transducers and to remove the borehole voids.

The piezoelectric transducers operate by converting a transient elastic wave into an electric signal or vice versa. The monitoring system is then operated in one of two modes. The first is used to passively monitor AE activity preferentially within the array volume. AEs release elastic energy in the same way as 'earthquakes' but over a very small scale. At these frequencies AEs have a moment magnitude (M_w) of approximately –6. They occur either during the creation process of new fractures within the medium, or on pre-existing fractures due to small scale movements. Each receiver has a frequency response of approximately 35–350 kHz and contains a 40 dB pre-amplifier. This minimises a reduction in signal-to-noise between the sensors and the acquisition system. The sensors have a vulcanised surround and a high pressure reinforced cable to protect them from water infiltration. In addition, polyamide tubes and *Swagelok* connectors have been fitted to the cables to reduce the likelihood of breakage.

Figure A2-1. *Top: Schematic diagram of the locations of all transducers on a single frame. Left: Photo of a section of the transducer assembly. Right: Transducer assembly during installation.*

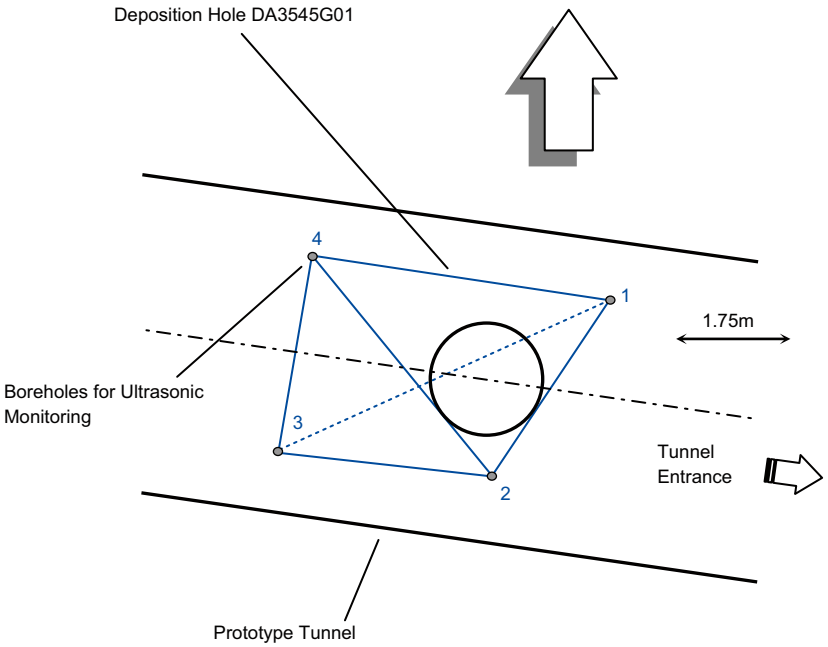

Figure A2-2. *Plan view of the array geometry for Deposition Hole DA3545G01 during heating in the Prototype Tunnel. The blue solid lines represent direct ray-paths between sondes illustrating their 'skimming' nature. The blue dashed line represents a ray-path that travels through the deposition hole.*

Table A2-1. Boreholes used for AE monitoring of deposition hole DA3545G01.

SKB Borehole designation	ASC Borehole reference	Transducer Numbers
KA3543G01	1	T1, T2, R1–R4
KA3545G02	2	T3, T4, R5–R8
KA3548G03	3	T5, T6, R9–R12
KA3548G02	4	T7, T8, R13–R16

Figure A2-3 shows a schematic diagram of the acquisition system used. Cables from each transducer pass through the pillar between the PRT and the G-tunnel. Data acquisition uses a Hyperion Ultrasonic System controlled by a PC, set up within a cabin provided by SKB. This has 16 receiving channels and 8 transmitting channels. An AE is recorded when the amplitude of the signal on a specified number of channels exceeds a trigger threshold within a time window of 5 ms. The system then records the full-waveform signals from all 16 transducers. In this case a trigger threshold of 50 mV on three channels was used. This allows the system to have sufficient sensitivity to record high quality data without recording an abundance of activity that cannot be processed due to very small signal to noise on only a few channels. The captured signals are digitised with a sampling interval of 1 μs and a total length of 4,096 data points. In general, low noise levels were observed (< 2 mV) giving high signal to noise and good quality data. AE monitoring is set to switch off during daytime working hours (6 am–8 pm) so as to minimise the amount of noise recorded from human activity.

A second operating mode actively acquires ultrasonic waveforms by scanning across the volume. This allows measurements of P- and S-wave velocities and signal amplitudes over a possible 128 different ray-paths. By repeating these ultrasonic surveys at increments in time, a temporal analysis is obtained for the variation in medium properties. Ultrasonic surveys are conducted daily at 1 am in order to measure changes in P- and S-wave signals. At that time of night, no human activity will cause noise that can interfere with the signals received. A Panametrics signal generator is used to produce a high frequency electric spike. This is sent to each of the 8 transmitters in turn. The signal emitted from each transmitter is recorded over the 16 receivers in a similar fashion to that described above. An external trigger pulse from the signal generator is used to trigger the acquisition system and identifies the transmission start time to an accuracy of one sample point. In order to decrease random noise the signal from each transmitter is stacked 100 times.

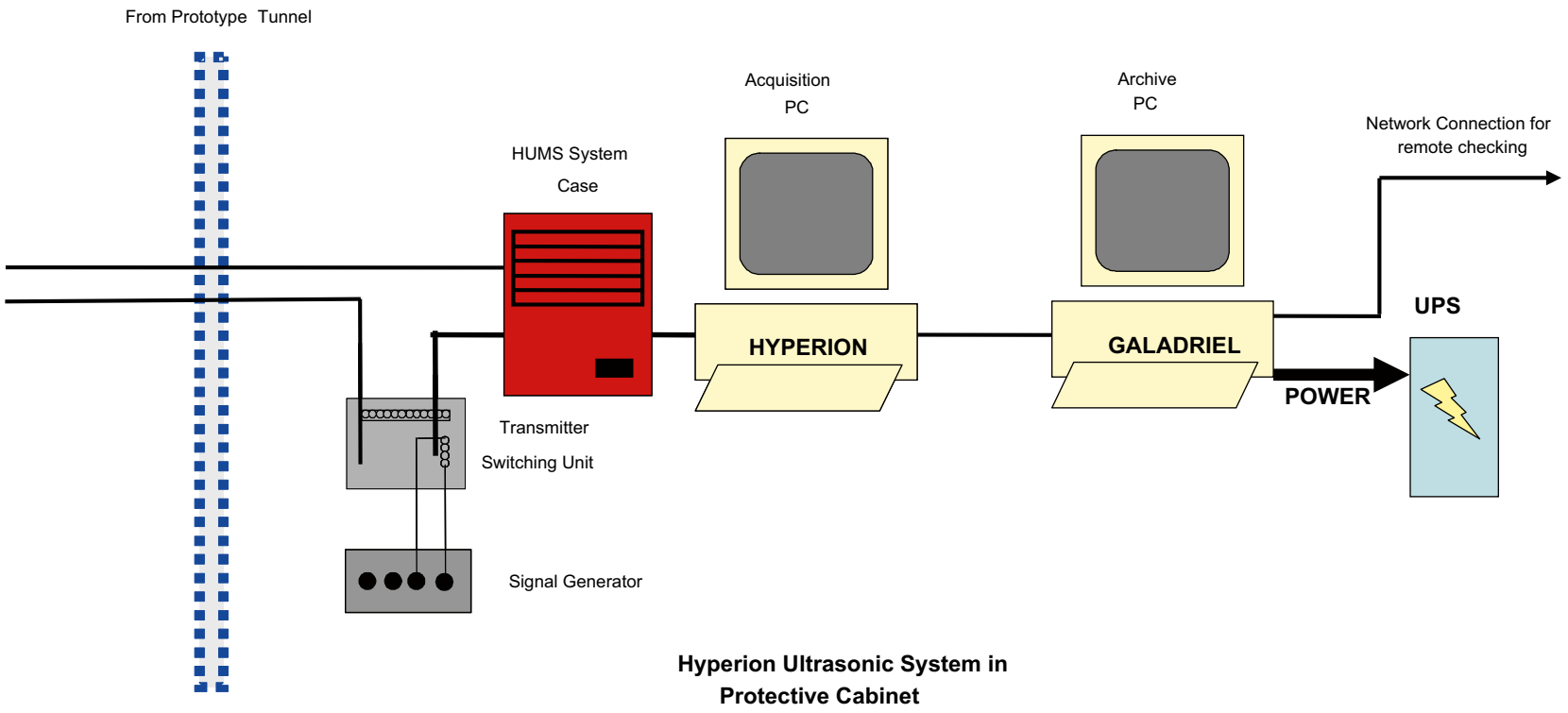

Figure A2-3. *Schematic diagram of the hardware used for the heating stage in the Prototype Repository. The ultrasonic pulse generator sends a signal to each transmitter and the resulting signal is recorded on each receiver. The receivers are also used to listen for AE activity. The archive PC is required to make a copy of the data for backup purposes.*

Processing procedure

Overview

ASC's InSite Seismic Processor has been used to automatically process both the AE and ultrasonic survey data. Appendix 3A and Appendix 3B give the processing parameters used. Pettitt and Young (2007) provides a detailed description of this software.

Ultrasonic data procedure

The ultrasonic survey full-waveform data was initially stored with the AE data. This was automatically sorted and the survey data extracted to a separate processing project. For pervious processing, a reference survey recorded on 8th December 2004 and has had first P- and S-wave arrivals manually picked from the waveform (Haycox and Pettitt 2006a). After refurbishment of the acquisition system in November 2008 it has been observed that a new reference survey is required in the processing due to changes in signal amplitudes. The characteristics of recorded waveforms from the 8th December 2004 reference survey and 28th November 2008 survey have been evaluated and show that they were generally similar, but following the refurbishment and reinstallation of the equipment the amplitudes of the waveforms have generally increased. This new reference survey has been imported into the project and used to process the ultrasonic results. Since transmitter and receiver locations are known, the ultrasonic velocity for each ray-path can be calculated with an estimated uncertainty of $\pm$ 30 ms^{-1} ($\pm$ 3 data points). Cross-correlation can then be used to automatically process subsequent surveys. This technique cross-correlates P- and S-wave arrivals from a transmitter-receiver pair with arrivals recorded on the same transmitter-receiver pair from the reference survey. Note that when the transmitter and receiver are on the same borehole, the ray-path is not used due to the introduction of transmission effects from the instrumentation borehole, grout and transducer frames.

Manual picking of arrivals by the examiner can often be erroneous due to random noise superimposed on the first few data points of the first break. By using the cross-correlation procedure it reduces this uncertainty and allows high-resolution analysis, with an estimated uncertainties of $\pm$ 2 ms^{-1} between surveys on individual ray-paths, to be performed and hence small changes in velocity to be observed. This is extremely important when changes in rock properties occur over only a small section (~5%) of the ray-path.

Figure 4-7 gives example waveforms recorded from one of the transmitters. Each waveform is first automatically picked to obtain an estimate of the P-wave or S-wave arrival. A window is then automatically defined around the arrival and a bell function is applied, centred on the automatic pick. The data at the ends of the window then have a much smaller effect on the cross-correlation. The windowed data are then cross-correlated (Telford et al. 1990) with a similar window constructed around the arrival on the reference survey. The change in arrival time is then converted to a change in velocity knowing the manually-picked arrival time for the reference survey. Waveforms that do not provide automatic picks are not cross-correlated. This gives an automatic discrimination of signals that have very poor signal to noise ratios and could give spurious cross-correlation results from poor discrimination of the first arrival. During the automatic processing, an arrival amplitude is also calculated from within a processing window defined by a minimum and maximum transmission velocity. This provides a robust measure of arrival amplitudes between surveys.

When calculating average velocities and amplitudes, ray-paths passing through the deposition hole are removed due to the uncertain transmission paths produced by the wave travelling in the rock around the deposition hole and through the bentonite, fluid and canister fill. Therefore the majority of ray-paths between boreholes 1 and 3 (transmitters 1, 2, 5, 6 and receivers 1, 2, 3, 4) are not used in the analysis. An exception is made for the deepest ray-paths that pass under the deposition hole entirely through rock.

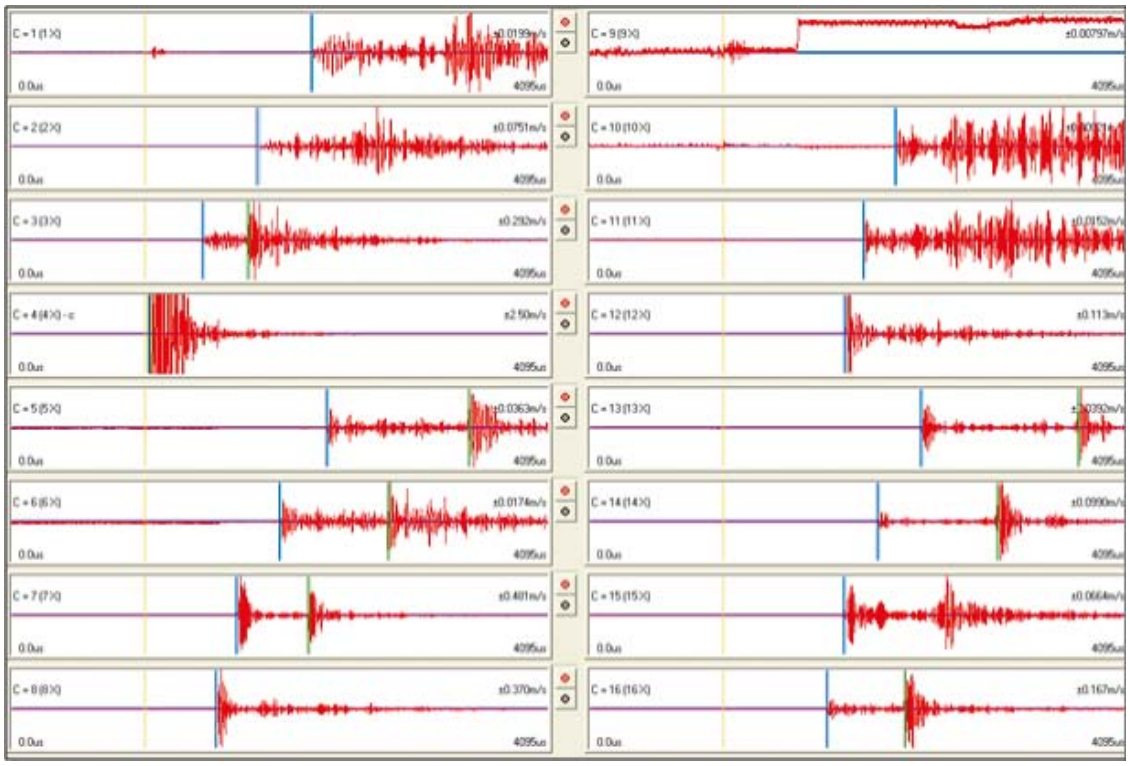

Figure A2-4. *Waveforms recorded from one transmitter on the array of sixteen receivers. The gold markers indicate the transmission time. The blue and green markers indicate picked P- and S-wave arrivals respectively.*

The dynamic Young's modulus E, and dynamic Poisson's Ratio, σ, can be calculated from the velocity measurements using Equation A2-1 and Equation A2-2.

$$E = \rho V_S^{\,2}\left(\frac{3V_P^{\,2} - 4V_S^{\,2}}{V_P^{\,2} - V_S^{\,2}}\right) \tag{A2-1}$$

$$\sigma = \frac{V_P^{\,2} - 2V_S^{\,2}}{2\left(V_P^{\,2} - V_S^{\,2}\right)} \tag{A2-2}$$

V_P and V_S values are also used to model for crack density (c) and saturation (s) in the rock mass using the method of Zimmerman and King (1985). The crack density parameter is defined by the number of cracks (penny-shaped) per unit volume multiplied by the mean value of the cube of the crack radius (Equation A2-3). This method assumes the elastic modulus E and σ in the damaged material normalized to the undisturbed material, decrease exponentially with crack density. Also assumed are the shear modulus (μ) is unaffected by s, and the bulk modulus (k) increases linearly with s, equalling that of uncracked rock when s=1. Equation A2-4 shows the calculation used to determine saturation.

$$c = \frac{9}{16}\ln\left(\frac{2\mu}{E_0 - 2\mu v_0}\right) \tag{A2-3}$$

$$s = \frac{k(c,s) - k(c,0)}{k_0 - k(c,0)} \tag{A2-4}$$

The calculations require an estimation of the completely undisturbed rock (i.e. an unsaturated, uncracked and intact rock mass). This study assumes values of V_{0P} = 6,660 ms^{-1}, and V_{0S} = 3,840 ms^{-1} for the undisturbed material taken from laboratory tests on a similar granite, summarized in Maxwell and Young (1995). A value of 2,650 kg m^{-3} is presented by Pettitt et al. (2002) for the density of the rock mass.

Young's Modulus and Poisson's ratio are calculated from measured velocities by making the assumption that the transmission medium is isotropic elastic. Under this assumption a rock can be completely characterised by two independent constants. One case of an isotropic elastic medium is a rock with a random distribution of cracks embedded in an isotropic mineral matrix. Under the application of a hydrostatic compressive stress, the rock will stay isotropic but become stiffer (characterised by increased velocity (V_P and V_S) and therefore increased Young's Modulus). In contrast, under the application of a uniaxial compressive stress, cracks with 'normals' parallel or nearly parallel to the applied stress will preferentially close and the rock will take on a transversely isotropic symmetry. Under this situation P- and S-wave velocities become variable with orientation. The crack density and saturation calculations also assume an isotropic elastic medium.

It should be noted that E and σ calculated in this report are dynamic measurements due to the small strains exerted on the rock mass at high frequencies from the passing ultrasonic waves. Static E and σ measurements, made from uniaxial laboratory tests on rock samples, may be different from dynamic values – even if sample disturbance is minimal – due to the larger strains exerted over relatively long periods of time.

Acoustic emission procedure

The procedure used to process the AEs in this monitoring period has been undertaken as follows:

1. Calibration surveys from the installation phase (when the deposition hole was open) have been used to optimise an automatic picking and source location algorithm and check location uncertainties. ASC's InSite seismic processing software was used for location and visualisation.
2. Where possible, P- and S-wave arrival times were measured for each AE using the automatic picking procedure.
3. AEs with ≥ 6 P-wave arrival times were input into a downhill-simplex location algorithm (Pettitt and Young 2007). This has the option of incorporating either a three-dimensional anisotropic velocity structure or an isotropic structure. Velocities calculated from the ultrasonic surveys were used.
4. The waveforms from all events were visually inspected to ensure they were 'real' acoustic emissions. Events were removed if they had the appearance of noise spikes (increase in amplitude is recorded on all channels at the same time) or they were the result of human noise (long period events that occur at close intervals during the day).
5. The acoustic emissions that remained had their arrivals manually picked to obtain the best possible location. Any events that located outside the expected region of activity were further checked to ensure accuracy. Experience from previous studies around deposition holes showed that large source location errors were produced if significant portions of a ray-path passed through the excavated deposition hole void. This only becomes a problem for the largest AEs. AEs were reprocessed with these ray-paths removed.
6. Finally, a filter was applied to remove all AEs with a location error greater than 1.0.

During the equipment installation phase, calibration shots were undertaken to assess the sensitivity of the system to AEs and to determine the accuracy with which real events could be located by the array of sensors. A series of tests, called 'shots', were performed on the wall of deposition hole DA3545G01 (Figure A2-5). The shots consisted of undertaking 10 'pencil lead breaks' and 10 hits with a screw-driver at 1 metre intervals down 4 lines along the wall of the deposition hole. The pencil-lead tests involved breaking the 0.5 mm lead from a mechanical pencil against the borehole wall. This is a 'standard' analogue for an AE as it generates a similar amount of high-frequency energy. An example of a pencil lead break test is shown in Figure A2-6. This was made at 6 metres below the tunnel surface on the wall of the deposition at a point adjacent to borehole KA3548G02. This corresponds to an AE source dimension on the millimetre scale (grain size).

The screw-driver hits provided a good amplitude signal for assessing the accuracy with which events can be located within the volume surrounded by the array. Figure A2-5 shows the results from one processed set of locations for a line of shots down the deposition hole. This shows that the array is able to locate events with good accuracy and consistency within an estimated uncertainty of approximately 10 cm.

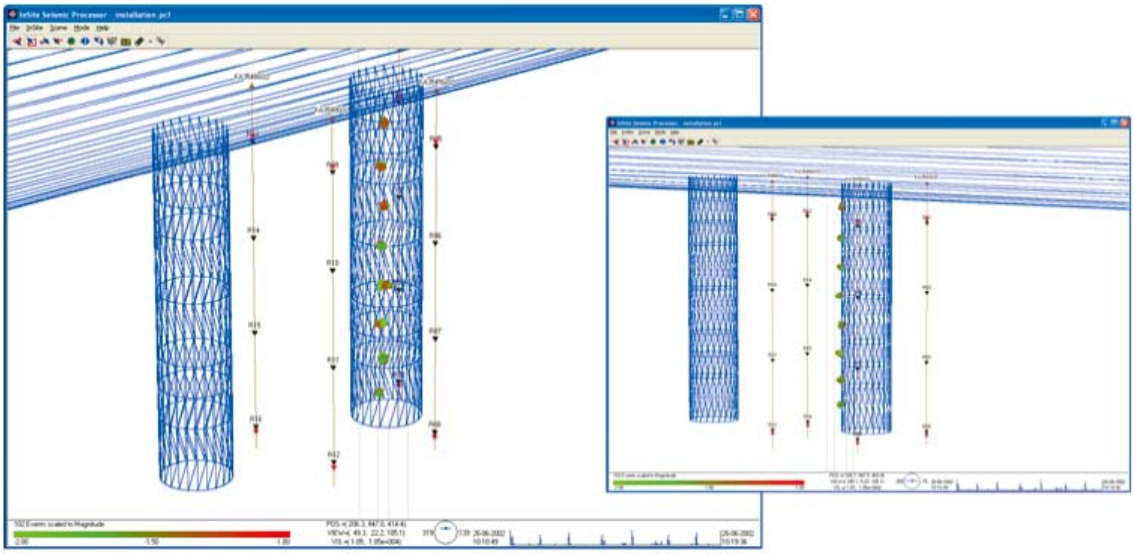

Figure A2-5. *Locations of calibration shots obtained from a series of tests at 1 metre intervals down the wall of deposition hole DA3545G01. The two views show that these line up and are located close to the surface of the hole.*

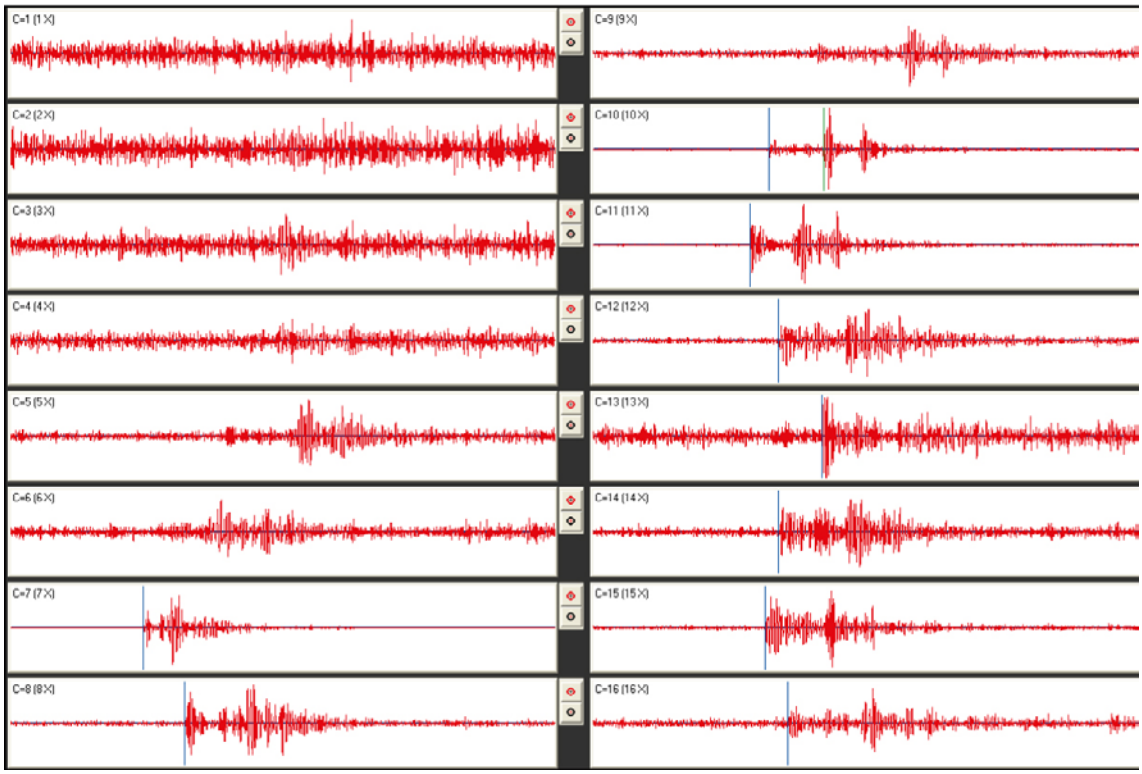

Figure A2-6. *Example waveforms from each of the 16 receiving channels for a 'pencil-lead break' test undertaken against the Deposition Hole (DA3545G01) wall 6 metres below the tunnel floor.*

Appendix 3

Processing parameters

A: Ultrasonic survey processing parameters:

Proccessing parameters	Velocity survey processing
Event initialisation	
View/process waveforms by	Channel
Channel-view Width-to-height ratio	6
Waveform Response type	Set from sensor
Sampling time	1
Time units	Microseconds
Pre-signal points	200
Spline sampling time	0.2
Waveform To point	1,023
P-Time correction	0
S-Time correction	0
Automatically update Channel Settings	NOT SET
Project Files	NULL
Auto picking	
Allow P-wave Autopicking	YES, Use first peak in the auto-pick function
Back-window length	100
Front-window length	35
Picking Threshold	4
Min. Peak-to-Peak amplitude	0
Allow S-Wave Autopicking	YES, Use first peak in the auto-pick function
Back-window length	100
Front-window length	35
Picking Threshold	3
Min. Peak-to-Peak amplitude	0
Allow Automatic Amplitude Picking	YES
Use Velocity Window Picking	YES
P-wave Min. Velocity/Max. Velocity	4,500, 6,500
S-wave Min. Velocity/Max. Velocity	2,500, 3,500
Cross-correlation	
CCR Events	Referenced to a Survey
Reference Component	20081128010037
Reference Event	NULL
Window construction method	Front to Back
Window comparison method	Fixed to reference picks
Window Parameters	Back-window length = 20
	Front-window length = 30
	Rise-time multiplier = NULL
	Power to raise waveform = 1
	Split to a Spline function = YES
	Obtain absolute waveform = NOT SET

Locater	(not used in velocity surveys)
Method	SIMPLEX INTO GEIGER
Method settings	Tolerance = 0.01
Simplex settings	LPNorm = 1
	P-wave weighting = 1
	S-wave weighting = 1
	Use Outlier Identification = NOT SET
	Arrival error factor = ×2
Geiger settings	Tolerance (Loc. units) = 0.01
	Step size (Loc.units) = 0.1
	Max. Iterations = 100
	Conditional No. Limit = 10,000,000,000
Velocity Structure	Homogeneous Isotropic
Velocity Structure settings	P-wave velocity = 6,000 ms^{-1}
	S-wave velocity = 3,350 ms^{-1}
	Attenuation = 200
	Q(S) value = 100
Data to use	P-wave Arrivals Only
Distance units	Metres
Working time units	Microseconds
Min P-wave arrivals	0
Min S-wave arrivals	0
Min Independent arrivals	5
Max. Residual	20
Start point	Start at the centroid of the array
Write report to RPT	NOT SET
Source parameters	Set to calculate automatically

B: AE processing parameters:

Proccessing parameters	AE processing
Event initialisation	
View/process waveforms by	Channel
Channel-view Width-to-height ratio	6
Waveform Response type	Set from sensor
Sampling time	1
Time units	Microseconds
Pre-signal points	200
Spline sampling time	0.2
Waveform To point	1,023
P-Time correction	0
S-Time correction	0
Automatically update Channel Settings	SET
Project Files	NULL
Auto picking	
Allow P-wave-autopicking	YES, Use max peak in the auto-pick function
Back-window length	100
Front-window length	35
Picking Threshold	5
Min. Peak-to-Peak amplitude	0

Auto picking	
Allow S-Wave Autopicking	YES, Use max peak in the auto-pick function
Back-window length	100
Front-window length	35
Picking Threshold	5
Min. Peak-to-Peak amplitude	0
Allow Automatic Amplitude Picking	NOT SET
Use Velocity Window Picking	YES
P-wave Min. Velocity/Max. Velocity	4,500, 6,500
S-wave Min. Velocity/Max. Velocity	2,500, 3,500

Cross-correlation	**(not used in AE processing)**
CCR Events	NOT SET
Reference Component	NOT SET
Reference Event	NULL (not activated)
Window construction method	Individual
Window comparison method	Fixed to reference picks
Window Parameters	Back-window length = 20
	Front-window length = 30
	Rise-time multiplier = NULL
	Power to raise waveform = 1
	Split to a Spline function = NOT SET
	Obtain absolute waveform = NOT SET

Locater	
Method	SIMPLEX INTO GEIGER
Method settings	Tolerance = 0.01
Simplex settings	LPNorm = 1
	P-wave weighting = 1
	S-wave weighting = 1
	Use Outlier Identification = NOT SET
	Arrival error factor = ×2
Geiger settings	Tolerance (Loc. units) = 0.01
	Step size (Loc.units) = 0.1
	Max. Iterations = 100
	Conditional No. Limit = 10,000,000,000
Velocity Structure	Homogeneous Isotropic
Velocity Structure settings	P-wave velocity = 5,983.9 ms^{-1}
	S-wave velocity = 3,344.4 ms^{-1}
	Attenuation = 200
	Q(S) value = 100
Data to use	P-wave Arrivals Only
Distance units	Metres
Working time units	Microseconds
Min P-wave arrivals	0
Min S-wave arrivals	0
Min Independent arrivals	5
Max. Residual	20
Start point	Start at the centroid of the array
Write report to RPT	NOT SET
Source parameters	Set to calculate automatically

Event filter	
Date and Time	NOT SET
Location volume	Minimum = (235, 880, 420)
	Maximum = (300, 964, 463)
L. Magnitude	NOT SET
Location Error	1
Independent Instruments	Minimum = 0

Source parameters	
Automatic source-parameter windows	P-wave back window = 10
	P-wave front window = 50
	S-wave back window = 10
	S-wave front window = 50
Source parameter calculations	Min number to use = 3
Automatic source-parameter windows	Apply Q correction = SET
	Source density = 2,640
	Source shear modulus = 39,131,400,000
	Av. radiation coefficient: Fp = 0.52, Fs = 0.63
Source parameter calculations	Source coefficient: kp = 2.01, ks = 1.32
Magnitude calculations	Instrument magnitude = 1 × log (ppV) +0
	Moment magnitude = 0.666667 × log(Mo) + –6